İSTANBUL TECHNICAL UNIVERSITY ★ GRADUATE SCHOOL OF SCIENCE ENGINEERING AND TECHNOLOGY

INVESTIGATION OF URBAN HEAT ISLAND INTENSITY AND DEVELOPING MITIGATION STRATEGIES FOR ISTANBUL

M.Sc. THESIS

Simge İrem BİLGEN

Department of Meteorological Engineering

Atmospheric Sciences Programme

JUNE 2016

İSTANBUL TECHNICAL UNIVERSITY ★ GRADUATE SCHOOL OF SCIENCE ENGINEERING AND TECHNOLOGY

INVESTIGATION OF URBAN HEAT ISLAND INTENSITY AND DEVELOPING MITIGATION STRATEGIES FOR ISTANBUL

M.Sc. THESIS

Simge İrem BİLGEN
(511131030)

Department of Meteorological Engineering

Atmospheric Sciences Programme

Thesis Advisor: Prof. Dr. Yurdanur S. UNAL

JUNE 2016

İSTANBUL TEKNİK ÜNİVERSİTESİ ★ FEN BİLİMLERİ ENSTİTÜSÜ

İSTANBUL İÇİN ŞEHİR ISI ADASI ŞİDDETİNİN ARAŞTIRILMASI VE AZALTMA STRATEJİLERİNİN GELİŞTİRİLMESİ

YÜKSEK LİSANS TEZİ

Simge İrem BİLGEN
(511131030)

Meteoroloji Mühendisliği Anabilim Dalı

Atmosfer Bilimleri Programı

Tez Danışmanı: Prof. Dr. Yurdanur S. ÜNAL

HAZİRAN 2016

Simge İrem Bilgen, a M.Sc. student of İTU Graduate School of Science Engineering and Technology student ID 511131030, successfully defended the thesis/dissertation entitled **"INVESTIGATION OF URBAN HEAT ISLAND INTENSITY IN ISTANBUL"**, which she prepared after fulfilling the requirements specified in the associated legislations, before the jury whose signatures are below.

Thesis Advisor :	**Prof. Dr. Yurdanur S. UNAL** İstanbul Technical University	....
Jury Members :	**Prof. Dr. Sahar SODOUDI** Freie Universität Berlin	....
	Prof. Dr. Sema TOPÇU İstanbul Technical University	....

Date of Submission : 02 May 2016
Date of Defense : 16 June 2016

To my family,

FOREWORD

This is the M.Sc. thesis completed as a requirement of Department of Meteorology Engineering Atmospheric Sciences Program at Istanbul Technical University. In this project, in order to investigate what type of changes in the urban landscape elevate the intensity of UHI in Istanbul some mitigation strategies are applied and reducing the the intensity is aimed. I am very grateful to my advisor Prof. Dr. Yurdanur S. UNAL for being so patient and tolerant to me during thesis period.
I would like to extend my thanks to Prof. Dr. Sahar SODOUDI, Ahmet Ozgur DOGRU and CANER GUNEY and also to Cemre YURUK, Deniz DIREN, Nur GOKTEPE, ERKAN YILMAZ and FULDEN BATIBENIZ for supporting me every time. Finally, I thank to my family for encouraging and always being with me.

June 2016

Simge İrem BİLGEN
(Meteorological Engineer)

TABLE OF CONTENTS

Page

ABBREVIATIONS

ASCII	**:** American Standard Code for Information Interchange
BATS	**:** Biosphere Atmosphere Transfer Scheme
CEST	**:** Central European Summer Time
CORINE	**:** Coordination Of Information On The Environment
DCC	**:** Disaster Coordination Center
DWD	**:** German Meteorology Service (Deutsch Wetterdienst)
GCM	**:** General Circulation Model
GIS	**:** Geographic Information System
IBB / IMM	**:** Istanbul Metropolitan Municipality
IPCC	**:** Intergovernmental Panel on Climate Change
LAI	**:** Leaf Area Index
LUTAB	**:** Land Use Table
MOST	**:** Monin-Obukhov Similarity Theory
MUKLIMO	**:** Micro-Scale Urban Climate Model
OMEGA	**:** Operational Multiscale Environment model with Grid Adaptivity
RCP	**:** Representative Concentration Pathways
TSMS	**:** Turkish State Meteorological Service
UHI	**:** Urban Heat Island
UHII	**:** Urban Heat Island Intensity
UTC	**:** Coordinated Universal Time
WD	**:** Wind Direction
WS	**:** Wind Speed
1D	**:** One Dimensional
3D	**:** Three Dimensional

SYMBOLS

$\boldsymbol{H_b}$	: Mean Building Height
$\boldsymbol{H_t}$	: Mean Height ofTrees
$\bar{\boldsymbol{g}}$	: Three Dimensional Constant
$\boldsymbol{j^c}$	: The Diffusion Flux
$\boldsymbol{j^q}$	: Turbulent Heat Flux
$\bar{\boldsymbol{J}}$	: Stress Tensor
$\boldsymbol{K_h}$	: The Exchange Coefficient for Heat
$\boldsymbol{K_m}$	: Turbulent Exchange Coefficient for Momentum
$\boldsymbol{l}$	: Mixing Length
$\boldsymbol{Lai_c}$	: Leaf Area Index of the Canopy Layer
$\boldsymbol{Lai_t}$	: Leaf Area Index of the Trees
$\boldsymbol{Q}$	: Anthropogenic Heat Production
$\boldsymbol{Q^c}$	: Volume Source of C
$\boldsymbol{Q_e}$	: Latent Heat Flux
$\boldsymbol{Q_h}$	: Sensible Heat Flux
$\boldsymbol{rh}$	: Relative Humidity
$\boldsymbol{Ri}$	: Richardson Number
$\boldsymbol{T}$	: Air Temperature
$\boldsymbol{\Sigma_t}$	: Fraction of Tree Cover
$\boldsymbol{V}$	: Fraction of Pavement of the Non-Built Area
$\vec{\boldsymbol{v}}$	: Stream Velocity
$\boldsymbol{W_b}$	: Wall Area Index
$\boldsymbol{y}$	: Horizontal Wind Vector
$\boldsymbol{\Gamma_b}$	: Fraction of Built-Up Area
$\boldsymbol{\rho_o}$	: Constant Mean Values of the Density
$\boldsymbol{\theta_o}$	: Constant Mean Values of the Potential Temperature
$\vec{\boldsymbol{\Omega}}$	: Angular Velocity
$\bar{\boldsymbol{\Psi}}$	: A Vector Potential or Vector Stream Function
$\boldsymbol{\xi}$	: The Vectorial Vorticity
$\boldsymbol{\nabla p}$	: The Wind Field
$\boldsymbol{\Phi(Ri)}$	: Stability Function

LIST OF TABLES

Page

LIST OF FIGURES

Page

INVESTIGATION OF URBAN HEAT ISLAND INTENSITY AND DEVELOPING MITIGATION STRATEGIES FOR ISTANBUL

SUMMARY

Urbanization and climate change may be the two most significant socio-ecological issues of the 21st century. The intersection between these trends is intensified by increasing population. Thus, the quality of life is influenced negatively. Cities are the defining ecological phenomenon in the decades ahead and the majority of the population of world now lives in them (While and Whitehead, 2013).

Significant urbanization has occurred in Istanbul due to incerase of the population. Urban growth and associated landscape transformation might be a major driver of local and regional environmental change in this city. Istanbul is the largest city of Turkey with the population over 14 million inhabitants and the urbanization is drastically expanded since 1965 due to the population increase from 2 million to 14 million.

As long as cities proceed to grow and develop with climate change, in order to mitigate urban temperatures by identifying and assessing practical strategies, is critical to provide socio-ecological urban sustainability and thermal comfort (Coutts et al. 2013). Using green and cool (high-albedo material) roofs are commonly reported to provide urban heat mitigation potential; however, their performance is highly dependent upon their design, sunshine duration, and location of the built-up area. This study compares the role of land use and wind field modifications to alter the urban climate in Istanbul by modeling spatial distribution of the urban heat island given 33 mitigation strategies (including white, green and hybrid scenarios) and 10 sensitivity analyses (with wind speed and wind direction scenarios).

In this study, the impacts of urban expansion on meteorological variables in relation to the urban heat island (UHI) effect in Istanbul is investigated. To estimate the strength of UHI, the temperature differences between urban and suburban stations are calculated by using temperature observations from 6 stations for 1960-2014 years, and 34 stations for 2007–2012. In order to examine what type of changes in the urban landscape elevate the intensity of UHI in Istanbul, by using the dry days which were determined with the meteorological station data, the effects of change in land use on daytime and nighttime urban heat island (UHI) of Istanbul is examined using the micro-scale climate model MUKLIMO 3.

The model simulation for mitigation strategies takes place for 07.08.2012, which was the hottest day in a heat wave that lasted five days and exceeded 30.5°C (threshold value) from the 90th percentile of all six station’s data. A Case domain (Maslak) for date (07.08.2012) is selected and the implementation of green roofs and high-albedo materials are considered in order to lower the temperature. Due to the fact that MULIMO_3 provides the opportunity to implement green roofs as well as high-albedo materials in built-up areas easily, several mitigation strategies are applied.

The implementation of cool (high-albedo) materials for urban structures and green roofs as mitigation strategies in general show lower temperatures throughout the whole day, while the effects of white and hybrid scenarios are much higher than green roofs. For the roof treatments explored here, results suggest that cool roofs (white scenarios), provide the greatest overall benefit in terms of urban heat mitigation and energy transfer into buildings. The high albedo of the cool roof substantially reduced net radiation, leaving less energy available at the surface for sensible heating during the day. Under warm and sunny conditions, when soil moisture was limited, evapotranspiration from the green roof was low, leading to high sensible heat fluxes during the day. Irrigation improved the performance of the green roof by increasing evapotranspiration.

Consequently, the thermodynamic version of MUKLIMO_3 has decent skills to capture general pattern of urban climate parameters such as temperature, relative humidity and wind velocity. In order to evaluate the utilizability of mitigation strategies to reduce potential of heat stress, the results demonstrate suitable promise as a valuable tool for national stakeholders and urban climatologists. On the other hand, the rooftops of mega city Istanbul must be designed accordingly to target specific performance objectives, such as heat mitigation rather than receiver system or brick located roofs.

İSTANBUL İÇİN ŞEHİR ISI ADASI ŞİDDETİNİN ARAŞTIRILMASI VE AZALTMA STRATEJİLERİNİN GELİŞTİRİLMESİ

ÖZET

Bilinçsiz şehirleşme ve iklim değişikliği 21. yüzyılın en önemli sosyo-ekolojik sorunlarından biridir. Bu iki güncel konunun ortak sonuçları artan insan popülasyonu ile şiddetlenmekte, bune bağlı olarak da yaşam kalitesi de olumsuz etkilenmektedir. Özellikle son otuz yıldır şehirler ekolojik fenomenler olarak tanımlanmakta ve dünya nüfusunun büyük bir çoğunluğu artık kırsal alanlardansa şehirlerde yaşamayı tercih etmektedir (While and Whitehead, 2013).

İstanbul şehir merkezi ve çevresinde yaşayan 14 milyon insan ile Türkiye'nin en büyük şehridir. Bu mega kentteki insan popülasyonu 1965 yılında 2 miyon civarı iken %600'lük bir artış göstererek günümüzde 14 milyona ulaşmış; hızlı nüfus artışına bağlı olarak toplumun gereksinimlerini karşılamak üzere ortaya çıkan şehirleşme de, bu belirtilen periyot süresince şiddetli bir biçimde artmıştır.

Avrupa'daki birçok ülke nüfusundan fazla nüfusa sahip olan İstanbul'un konut ihtiyacını karşılayabilmek adına; birçok orman alanı, mesire yeri, yeşil alan, sit alanı yarım asırlık süre zarfında yerleşim alanine çevrilmiş, şehir dışında kalan yarı kırsal ve kırsal bölgeler de şehir sınırları içersine dahil edilmiş, şehir zaman içersinde büyümüş, daha geniş bit yüzölçümü kaplar hale gelmiştir. Bu da fiziksel, sosyal ve ekonomik süreçleri değiştirmiştir. Örneğin kontrolsüz şehirleşme trafiğin, düzensiz endüstrileşmenin ve düşük kalitede yerleşim alanlarının artışını tetiklemiş ve çevresel problemlerin ortaya çıkmasına veya şiddetlenmesine neden olmuştur.

Şehir alanlarında insan etkisi ile yaratılan değişiklikler şehir ortamında sıcaklıkların daha yüksek olmasına neden olmaktadır. Yeşil arazinin ve tarım alanlarının yerini beton yapıların alması ısının daha fazla absorplanmasını ve doğal olmayan yüzeylerden buharlaşmanın azalmasına neden olmakta, kentin enerji dengesi, yıllık ortalama yağış miktarı, kentin hakim rüzgar yönü ve ortalama rüzgar şiddeti gibi bir çok meteorolojik parametreyi değiştirmekte ve şehir ısı adası yaratmaktadır. Şehir ısı adası (UHI), şehir materyelleri ve yapılaşmanın çevresindeki havanın farklı ısınma ve soğuma oranlarının, lokal yüzey enerji dengesinden dolayı şehir yapıları ile onun çevresindeki sıcaklık farkı olarak tanımlanır. Başka bir deyişle şehir ısı adası, yeşil alanların azalması ve binalaşmanın artması sonucu şehir ortamı ile kırsal alan arasındaki sıcaklık farkıdır. Şehir alanları, genellikle şehir dışı mahalleler ve kırsal alanlara göre daha sıcaktır. Şehir/şehir dışı mahalleler ve kırsal koşullarda geniş yatay sıcaklık gradyanları meydana gelir. Şehir ısı adası indeksi yoğunluğu şehir-kırsal alan sıcaklık farkına bağlıdır ve genellikle yazın en fazladır.

İstanbul gibi yüksek büyüme oranları ile şehirleşen mega kentlerde şehirleşme, arazi kullanımında ve arazi örtüsünün özelliklerinde meydana gelen mevcut ağaçların kesilmesi, şehir alanlarının kenar mahallelerindeki bitki örtüsünün yok olması, yeni binaların yeni yolların yapılması ve diğer yapıların eklenmesi şeklinde önemli

değişiklikler sonucunda ortaya çıkmaktadır. Bu değişiklikler şehir ısı adasının (ŞIA) şiddetini arttırabilecektir. Şehir Isı Adasının (ŞIA) belirlenmesine yönelik bilimsel yazının sistematik incelemesi ve kullanılan yöntemlerin sorgulanması Stewart (2010)'un çalışmasında yer almaktadır. Şehir ısı adasına yönelik ilk bilimsel gözlemler 1833 yılında Luke Howard tarafından yazılmıştır (Stewart, 2011). Daha yeni bir çalışma olan Santamoris (2014) ŞIA konusundaki çalışmaları derlemiştir. Son yıllarda ŞIA etkisi, gözlemler ve sayısal modeller kullanılarak dünyadaki farklı bir çok büyük şehir için incelenmiştir. Örneğin, Giannaros (2013) sayısal modelleme ile Atina'nın gece sıcaklıklarının çevresindeki kırsal alanlara göre 4°C daha yüksek olduğunu göstermiştir. Velazquez-Lozada ve diğ. (2006) tropikal sahil şehri San Juan'daki ŞIA incelemiş ve bir yıla yakın simülasyonlar gerçekleştirmiştir. ŞIA çevre ve ekosistem üzerinde olumsuz etkiler yaratmaktadır. Sarrat ve diğ. (2006) ŞIA'nın Paris'teki bölgesel hava kirliliğine etkilerini incelemiştir.

Gelişmekte olan ülkelerdeki hızlı şehirleşme ve şehir nüfusundaki artış şehir ısı adasının etkilerini arttırmaktadır. Bu etki şehir planlamasında peyzaj dizaynına dikkat edilerek kısmen azaltılabilir. Bu etkiler bir çok bilimsel çalışmada değerlendirilmiştir (Susca ve diğ. 2011; Sun ve diğ., 2012). Susca ve diğ. (2011) New York şehrinde çok ölçekli yaklaşımla yeşil alanların pozitif etkilerini ortaya koymuştur. Sun ve diğ. (2012) Peking'de su alanlarının ŞIA etkilerini azaltmaya yardımcı olduğunu göstermiştir. Benzer olarak, Santamoris (2014) şehir ortamında su ile kaplı alanlara yer vermenin soğuk ada yarattığını ve bu nedenle ŞIA etkilerini azaltmak için şehir ortamında su alanların artırılmasını önermiştir.

ŞIA'nın bölgesel iklime etkisi daha önce bir çok çalışmada incelenmiştir. Örneğin, Lin ve diğ. (2008) Taipei, Kuzey Taiwan'daki ŞIA'nın bölgesel iklime etkisi konusunda çalışmış, ayrıca ŞIA'nın lokal sirkülasyonu değiştirerek deniz meltemini kuvvetlendirdiğini ve kara meltemini de zayıflattığını göstermiştir. Priyadarsini ve diğ. (2008) Singapur'daki ŞIA etkisini araştırmış ve düşük albedolu materyaller ve kuleler gibi ŞIA etkisine neden olan ana faktörleri ele almıştır. Vardoulakis ve diğ. (2013) de küçük bir Akdeniz şehrindeki 6°C'ye kadar olan saatlik yaz ŞIA şiddetini belirlemiş, ayrıca ŞIA yoğunlukları ve şehir havalandırması arasındaki ilişkiyi göstermiştir.

Unal ve diğ. (2013) Türkiye'nin batısı üzerindeki sıcak hava dalgası eğilimlerini incelemiş ve sıcak hava dalgası sayısı, uzunluğunun ve şiddetinin Batı Türkiye için artan eğilimde olduğunu ve bu değişimin güney enlemlerinde ve denizden uzak yerlerde kuvvetlendiğini göstermiştir. Bu, bölgedeki sirkülasyon değişiminin bir sonucu olabilir. Belirli bir tip sirkülasyon, İstanbul'daki sıcak hava dalgasının oluşumunu tetiklemiştir (Unal ve Menteş, 2006). Eğer, son birkaç yılda sirkülasyon tipinin frekansında bir artış olursa, İstanbul ŞIA etkisi ile güçlenen daha yüksek günlük sıcaklıklar ile karşılaşacaktır.

Sonuç olarak da kentsel büyüme ve buna bağlı arazi yapısında gerçekleştirilen değişikler, şehirdeki lokal ve bölgesel iklim değişimine neden olmaktadır. Lokal ikliminin değişmesi sonucu yoğun yerleşimin olduğu şehir merkezi sıcaklarında artış meydana gelmekte ve bu artış ekolojik kaynakların yanında yerleşik halkın sağlını ve refahını da etkilemeye başlamaktadır. Özellikle yaz sıcaklıklarında daha net gözlenen ve her geçen yıl da eksponansiyel olarak artan bu değişimler, şehir iklim değişikliği sorununu gündeme getirmektedir. Ancak, yüksek yaz sıcaklıklarını azaltmaya yönelik yapılan çalışmalar ve geliştirilen stratejiler ile, iklim değişiliği tehdidi altındaki büyümeye devam eden mega kentler için yaşanabilir şehir ortamı sağlanabilir (Coutts et al. 2013).

Bu çalışmada, İstanbul şehir ikliminde yüzey kullanım değişimi, şehir ısı adalarının mekansal dağılımı için verilen 7 değişim stratejisi ile modellenerek, şehir gelişim etkilerinin, meteorolojik değişkenlerin İstanbul'daki şehir ısı adaları üzerine olan etkisi incelenmiştir. Şehir ısı adalarının şiddetinin belirlenmesi için, şehir ve kırsal alandaki sıcaklık farklılığı 1960'dan 2013'e kadar 6 istasyon, 2007'den 2012' ye kadar 34 istasyondaki sıcaklık gözlemlerinden hesaplanmıştır.

Şehir ısı adalarının şiddetini, arazi kullanımındaki hangi değişkenlerin yükselttiğini belirlemek için, meteorolojik istasyonlardaki gözlemler ile kuru günler belirlenip, Alman Meteoroloji İşleri'nin (Deutsch Wetterdienst) geliştirdiği Mikro Ölçekli Şehir İklim Modeli olan MUKLIMO 3 ile İstanbul'daki şehir ısı adaları, yüzey kullanım değişiminin etkileri gece (minimum) ve gündüz (maksimum) sıcaklıkları için incelenmiştir. 6 meteoroloji istasyonundaki tüm verilerin yüzde 90'nı ile eşik değer 30.5°C belirlenmiş ve 5 gün süren sıcak hava dalgası için 07.08.2012 model simülasyonları için hedef gün seçilmiştir. Belirlenen tarih için yeşil çatı uygulamaları ve yüksek albedo materyelleri değiştirilerek, şehir ısı adası şiddetini düşük sıcaklıklara indirebilmek adına Maslak uygulama alanı seçilmiştir. MUCKLIMO 3 modeli seçilen 7 değişim stratejisi için şehirleşmedeki yüksek albedo yapılarını ve yeşil çatı uygulamalarını kolayca uygulanmasını sağlamıştır.

Sonuç olarak, MUKLIMO_3 modelinin termodinamik versiyonu şehir iklim parametrelerinin genel paternleri olan sıcaklık, bağıl nem ve rüzgar hızını iyi bir şekilde modellemeyi başarmıştır. Isı stres potansiyelini azaltmak için gelişim stratejilerinin kullanılabilirliğinin geliştirilmesi, paydaşlar ve şehir iklimcileri için değerli bir arayüzle uygun vaadleri sonuçlar bize sunmaktadır.

1. INTRODUCTION

Climate change is a global phenomenon for many years. Especially since the 1950s, many of the observed changes are unprecedented over decades to millennia. The atmosphere and ocean have warmed, the amounts of snow and ice have diminished, sea level has risen, the weather patterns have disturbed, and the concentrations of greenhouse gases have increased. In addition to these long-term changes in the climate system components, humans are affecting both the energy and water budget of the planet by changing the atmospheric composition and land use.

IPCC 2013 report indicates that all general circulation models (GCMs) estimate an increasing global air temperature for the future. Global surface temperature change at the end of the 21st century is likely to exceed 1.5°C relative to 1850 to 1900 for all RCP (the Representative Concentration Pathways) scenarios except RCP2.6. It is likely to exceed 2°C for RCP6.0 and RCP8.5, and more likely not to exceed 2°C for RCP4.5. This warming will continue beyond 2100 under all RCP scenarios except RCP2.6 (IPCC, 2013). Eventually, the number of days with thermal stress will increase in many regions of the world (Früh et al., 2010; Solomon et al., 2007). Not only enhanced discomfort but also a rise in fatality rate will be aggravated by the expected changes in strength and frequency of extreme daytime and nighttime temperatures (Souch and Grimmond, 2004). For instance, changes in many extreme weather and climate events have been observed since 1950s. It is very likely that the number of cold days has decreased while the number of warm days has increased on the global scale. Besides, the frequency of heat waves has increased in large parts of Europe, Asia and Australia (IPCC, 2014).

Urban areas are affected by the global warming and also key contributor to climate change. Metropolitan areas are the attraction centers for many people since they provide opportunities for better education, job and life style. Unfortunately, they greatly increase urban environmental problems such as air pollution, and energy consumption due to rapidly increasing urban population, especially in recent decades. Today, majority of the world population lives in urban areas whereas it was only 10% of the total population lived in the cities before the industrial. It is expected that urbanization will continue to rise in urban regions and the global population of cities will reach 66% by the year 2050 according to the United Nations Report (2014).

Urbanization leads to higher nocturnal temperature compared to surrounding rural areas, and the temperature difference between these urban areas and their surrounding due to the lack of green landscape and increasing built-up areas is defined as urban heat island (UHI). In urban areas, local climate conditions and high temperatures are caused by heat absorption in pavement, asphalt and concrete surfaces due to the decreased evaporative cooling. In a hot summer day, this stored heat is not released during daytime, since the buildings as well as the ambient air have high temperatures with small gradient in between. However, when the sun sets and the temperature of the atmosphere decreases, the heat start to be emitted from the build up areas and eventually, released heat heats the ambient air around the buildings causing higher nocturnal temperatures and this is known as heat island effect. The formation of UHI phenomenon depends upon the size and density of the population. According to Oke (1973), the urban heat island is directly proportional to the urban population. Cities are among those most jeopardized with the potential global climate change as the heat load in urban areas is expected to increase. Thus, urban climate research related to the global climate change has a vital importance for the inhabitants' welfare. Observing the possible range of heat load increase is indispensable, in terms of both its magnitude and intensity, for planning the mitigation strategies.

A systematic review and scientific critique of methodology in modern urban heat island literature has been made by Stewart (2010). According to Stewart (2010), first scientific observations on this phenomenon are performed and documented by Luke Howard (1833). Another successful review has been presented by Santamoris (2014). In the recent decade, UHI effect has been studied for the various cities specifically by using numerical modeling and well documented in the numerous papers. For example, Giannaros et al. (2013) showed by using numerical modeling that Athens exhibits 4.0K higher temperatures than its surroundings during night time.. Valesquez-Lozada et al. (2006) studied the UHI in the tropical coastal city of San Juan with numerical atmospheric modeling and presented the simulations up to year

2050. UHI has also negative impacts on urban-related environments and ecosystems located away from the cities. For example, Sarrat et al. (2006) examined the impact of UHI on regional atmospheric pollution over Paris region.

The effects of urban heat islands can be reduced by landscape design in urban planning(Susca et al. 2011; Sun and Chen, 2012; San et al. 2012). Susca et al. (2011) evaluated the positive effects of vegetation with a multi–scale approach in New York City. Sun and Chen (2012) suggested to increase water bodies to mitigate the UHI effects in Beijing. Furthermore, Santamoris (2014) has made a different suggestion such as urban cooling islands creating wetlands to mitigate UHI effects. The impact of UHI effect on regional climate has been examined by several papers. For example, Sodoudi et al. (2014) investigated the UHI characteristics of a megacity Tehran by using micro scale model and suggested some feasible mitigation strategies such as high albedo material, greenery on the surface and on the roofs and combination of them in order to reduce the air temperature and save energy. Lin et al. (2008) studied UHI effect on regional climate in Taipei, northern Taiwan. They also showed that UHI could enhance the sea breeze in the daytime and weaken the land breeze during the nighttime. Priyadarsini et al. (2008) investigated the UHI effect in Singapore and examine the key factors causing the UHI effect such as material having lower albedo, towers and street-canyons in this tropical city. Vardoulakis et al. (2013) determined hourly summer nocturnal UHI intensities in a small Mediterranean city up to 6.0K. He and his co-workers showed also significant relationship between UHI intensity and city ventilation. This causes higher cooling energy needs which is related with future climate change scenarios.

Istanbul is an ideal city for observing the urban heat island effect. There are several meteorological stations located throughout the city, is separated by Bosphorus, surrounded by two water bodies, Black Sea in the north and Sea of Marmara in the south, and apart from being the largest city of Turkey, it is also the fastest growing and most populated city (Karaca et al. 1995). Therefore, the local impacts of UHI effect in Istanbul has been investigated by the numerous papers. For instance, Karaca et al. (1995) studied the relationship between UHI intensity and population increase in Istanbul and also examined the fluctuations and trends that occurred in the climate of this mega city within the last four decades. Their study found that there is a warming trend in the minimum (nocturnal) temperatures for the southern part of the city where has high urbanization rate. In contrast, they also showed a cooling trend in the minimum temperatures for the less urbanized but more green northern part of Istanbul. Ezber et al. (2007) has shown that the urban heat island effect in Istanbul lead to local warming not only in the ambient nocturnal air temperature over the urban canopy but also in the low altitudes of atmosphere. In addition to atmospheric perturbation, this effect causes heating of underlying soil and rocks (Allen et al., 2003; Lee and Hahn, 2006). Yalcin and Yetemen (2009) investigated that the observations of the groundwater temperatures from the urban, southern part of Istanbul were 3.5K higher than the groundwater temperature from the rural, northern part of Istanbul and examined the possible UHI effect on the groundwater temperatures in urbanized areas of Istanbul. UHI has also impacts on local air circulation over the cities and this topic has been examined by Ezber et al. (2015). In this study, idealized case simulations by using non-hydrostatic mesoscale model, OMEGA (Operational Multiscale Environment model with Grid Adaptivity) are conducted in order to describe the contribution of sea–land breezes and UHI circulation to the local flow over Istanbul. They confirmed that the urbanized regions prevent the inland penetration of the sea breeze developing in the south by generating UHI circulation.

Cities are particularly influenced by the heat load related to global warming since this heat load adds to the well-known UHI effect (Früh et al. 2010). By reason of the diversity of towns the interaction between urban areas and the atmosphere is a complicated issue with many aspects (Sievers and Früh 2012). Besides, climate change strengthens the urban heat island over the cities and it will simultaneously influence more people in a negative way. This will cause enhanced stress conditions for the people living in urban, suburban and rural areas, respectively (Jendritzky, 2007). Particularly, heat-related events such as heat stroke, heat stress related deaths have potentially serious consequences for human health and assets. The assessment of the impact of climate change upon patterns of death and illness has been new research area on climate and health. Many studies have taken into consideration fatality rates during heat waves and under heat stress, and have found a positive correlation between heat and the number of deaths in all genders, ages and regions in the world (Ishigami et al., 2008; Harlan et al., 2012; Kovats and Hajat, 2008; Gabriel and Endlicher, 2011). There are several examples for the heat wave and its consequences in the world wide. The best known among of them is the European heat wave as an extreme climate anomaly occurred in the summer 2003, which was the warmest year since 1540. Europe’s 2003 heat wave has been extensively examined by Zaitchic et al. (2006). Most of them show evidence that heat stress effects more women and elder (Ishigami et al., 2008).

The formation of the urban heat island is caused by several factors, such as increasing built-up areas as well as the lack of vegetation. According to Sodoudi (2014), one of the most significant reasons of the UHI are the low albedo and the high heat capacity of roofs and walls such as concrete or asphalt, which absorb high amount of short-wave radiation during daytime, this energy is then slowly emitted during the nighttime as long-wave radiation from the walls and roofs and leads to higher air temperature in the cities. The other important reason of the formation of the urban heat island is the lack of green landscape of the cities. Urban areas have less evapotranspiration rate relative to natural landscapes, because of the lack of vegetation. This reduced moisture in built up areas cause to dry, impervious urban surface reaching very high surface temperatures, which contribute to higher air temperatures. Thus, using high albedo and greenery materials for walls and roofs can be useful mitigation strategies in order to reduce the urban heat island effect (Sodoudi, 2014). In a review of mitigation studies, green roofs are commonly assumed as a key approach for mitigating heat in urban areas according to Ayata et. al (2011) because of their thermal benefits, including the insulating effect of the vegetation (Gettler et. al., 2011). Chen and Wong (2009) found that green roofs could greatly decrease rooftop surface temperatures, also reducing ambient air temperatures. Likewise, cool roofs and walls (white surfaces) may also provide efficient mitigation of atmospheric heating and building energy savings through an increase in albedo (Rosenfeld, 1998; Synnefa, 2008).

The urban heat load in Istanbul has been increasing over the past decades since the urbanization has increased rapidly in the city particularly in the last 30 years. Istanbul is the largest city of Turkey in population, has been growing at a rate of 2.08 percent a year in recent decades. Due to the rapid increase of population in three decades, increased energy consumption and resultant changes in land use, uncontrolled urbanization have led to an overall environmental deterioration in this mega city. This study is first address the urban heat island intensity in Mega City

Istanbul and then investigates the role of land use modifications to modify the urban climate by modeling spatial distribution of the heat load. The reference land use dataset describes present urban structures as provided by both Istanbul Metropolitan Municipality and Basar Soft GIS (Geographic Information System), while the vegetation land use dataset is based on the digitalized geographical maps from the CORINE Land Cover. The long-period observational data from meteorological stations illustrate the magnitude and intensity of the urban heat load in the historical urban environment. Excluding the changes in the regional climate, it is possible to evaluate the urban bias originated by the city growth over 53 years. The work is proposed to clarify the complexity of the spatial signal related to the heat island formation and the response to the land use changes. It also validates the modeling approach to investigate trends in urban heat load and urban heat island on climatological time-scales, particularly useful for investigation of future development of the urban climate and long-term consequences of the urbanization.

In this work, a micro-scale urban climate model called MUKLIMO_3, which was developed by DWD (Deutscher Wetterdienst) is used and has not been validated sufficiently for Turkey until now. After adopting the model for Istanbul, creating current land use cover by using 3 different datasets and the implementation of several mitigation strategies, such as green roofs or the usage of high-albedo materials. In this way, MUKLIMO_3 may be a significant role in future projects, because many different combinations of these strategies and land use changes can be tested and the benefits can easily be compared against the costs of these strategies.

In order to maintain or enhance the quality of living in populated cities, urban climatologists and urban developers need comprehensive information on future urban climate on the residential area. The developers of the Microscale Urban Climate Model have developed an approximate but computationally inexpensive algorithm, which is called the cuboid method, to supply the data needed to estimate the impact of climate change on the urban heat load with the required resolution (Früh et al, 2010). The cuboid method is a statistical method to evaluate the number of extreme events in the future and present time slices and it reduce the computational effort induced by climatological analysis, in other words, this method allows one to simulate the load and the frequency of air temperature threshold exceedances such as hot days, heat waves, etc. with a less computational effort compared to the microscale simulations of the urban environment covering climatological time scales (30 yr) by using statistical downscaling approaches of regional climate model outputs in order to run the MUKLIMO_3. In so far as, this method might represent a useful downscaling technique for a wide range of applications. Nevertheless, using the model for Istanbul for the first time, in this work the cuboid method is not used, but will definitely be part of future work.

The aim of this thesis is to study the effects of greenery in connection with the high albedo materials in reducing the UHI effect in the metropolitan area of Istanbul and finding a mitigation strategy for adapting the infrastructure against the microclimate changes. This thesis is structured as follows. The background information about City of Istanbul is given in section 2. The data which are used in order to obtain the heat wave conditions of Istanbul from the TSMS (Turkish State Meteorological Service) and DCC (Disaster Coordination Center) Stations and the reference land use dataset provided by Istanbul Metropolitan Municipality and Basar Soft GIS (Geographic Information System) and CORINA Land Cover Data to create the current land use cover of Istanbul are presented in section 3. The description and the application of urban climate model and the land use cover of Istanbul is discussed in section 3. An evaluation of the micro-scale urban climate model, analyses and its results is presented in section 4. Closing statements are given in conclusion section 5.

2. MEGA CITY ISTANBUL

2.1 Topography

Istanbul is located at the north-western part of Turkey within the Marmara Region surrounded by seas on the north (Black Sea) and on the south (Marmara Sea). Continental Europe and Asia are separated by the Bosphorus and these sides currently connected with two bridges by the names of Boğaziçi and Fatih Sultan Mehmet. The new bridge on the north of the city is on construction in order to link these two sides for the third time. The western part of the city lays in the European continent and the eastern part in the Asian continent named as Anatolian side (Figure 2.1).

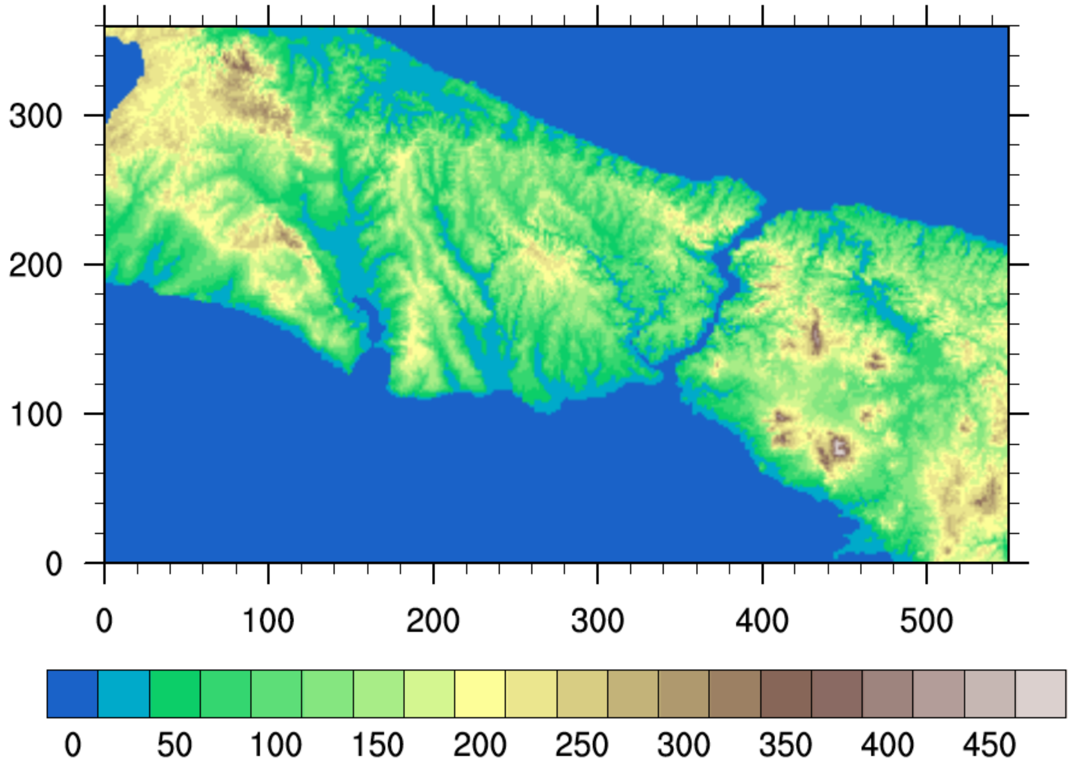

Figure 2.1 : Topography of Istanbul (height is given in meters).

The predominant wind directions of Istanbul are northeast and southwest. The city has also watersheds on the north part at both sides with about 117 km^2 area.

Topography and land cover distribution of Istanbul are shown in Figure 2.1 and Figure 2.2, respectively. The elevations at the northern parts of the city are higher compared to the southern parts. The highest elevations on the Asian side are Aydos and Çamlıca hills with the altitude of 537 and 268 meters above sea level, respectively. Figure 2.1 shows the situation of these hills in the large and densely populated Kartal and Üsküdar districts.

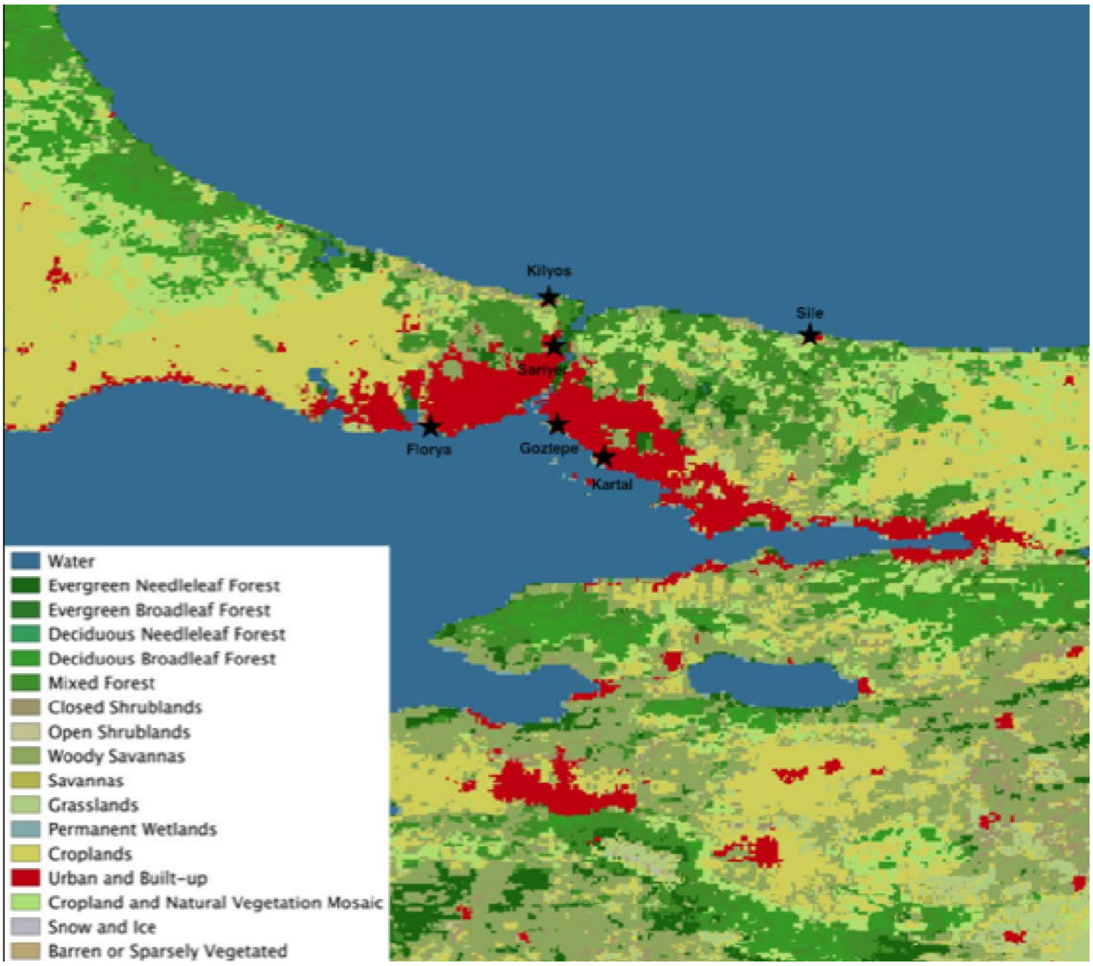

Figure 2.2 : Land cover distribution of Istanbul.

2.2 Urban Areas

The built-up areas are mostly located along the southern parts of Bosphorus and Marmara Sea coastline. Northern part of the city includes watersheds and covered by evergreen and deciduous forests (Figure 2.2). However, the expansion of the urban areas towards north, some of the forests have been already lost and also the implementation of the third Bosphorus bridge project which is still continuing, might result in further reduction of the city green areas.

Due to the rapid influx of population particularly in the last 30 years, the city faced uncontrolled urbanization which lead an overall environmental deterioration. According to previous researches, urbanized areas of Istanbul accounted for 751 km^2 in 2007 while it was 326 km^2 in 1987. It was increased more than double in 20 years. Hence it is expected that urbanized and urbanizing areas will exceed the 1/5 of the city areas in 2020. As the economic center and a 21st of megacity in the world, the city contributes itself well to the study of UHI and heatwaves.

2.3 Population

Istanbul is the fastest growing city with its economy and dense population not only in Turkey but also in Europe. Currently, it is one of the megacities in the world with about 15 million inhabitants and has an area of 5460 km^2 covering 39 districts (shown in Figure 2.3). Total area in the European part is 3,562 km^2 which is almost twice of the Anatolian Side as 1,897km^2 (IBB, 2015). Additionally, about 65% of the total population in the city lives in European part while 35% in Asian part.

Figure 2.3 : Districts of Istanbul (IBB, 2015)

Figure 2.4 illustrates the change of population in Istanbul since 1965 (TUIK, 2015). While the population was around 2 million in the 1965, it rapidly increased to more than 14 million in less than 50 years.

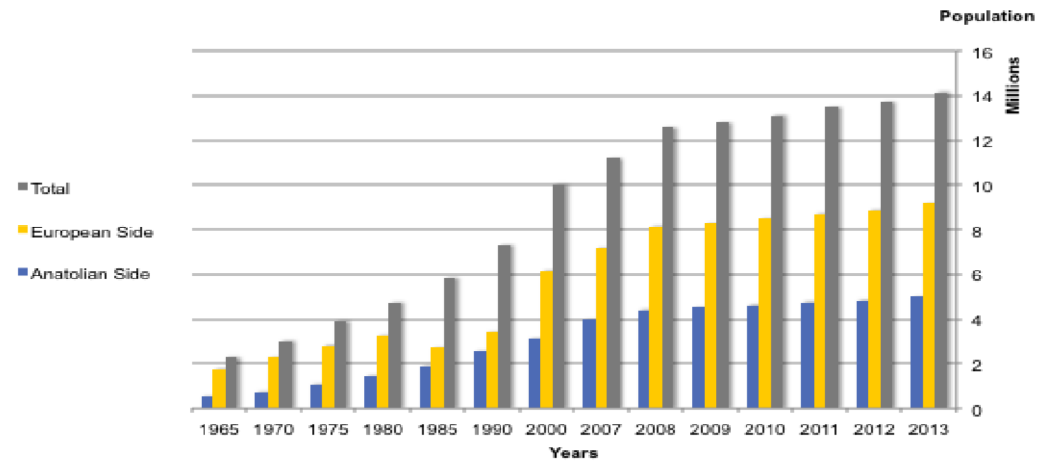

Figure 2.4 : Population change in Istanbul between 1965 and 2013.

Figure 2.5and Figure 2.6 demonstrate the population changes depending on the districts for Anatolian and European side of the city, respectively. Dense populated areas lie to the northwest, west and southwest on the European side, southwest on the Anatolian side. Kadıköy population was largest almost 10 years ago but due to the change of the province borders, the population seem to be dropped significantly within last decades. The provinces which has population over 500 thousand are Ümraniye, Pendik, Üsküdar and Kadıköy. On the European side, population of only two provinces is larger than 500 thousand, Bağcılar and Küçükçekmece.

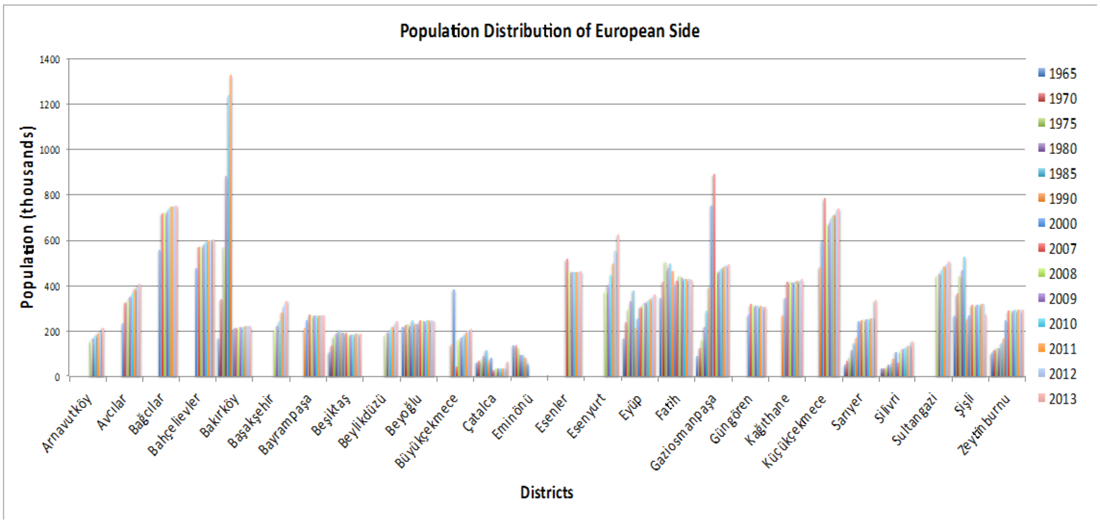

Figure 2.5 : Population change in European side of Istanbul between 1965 and 2013.

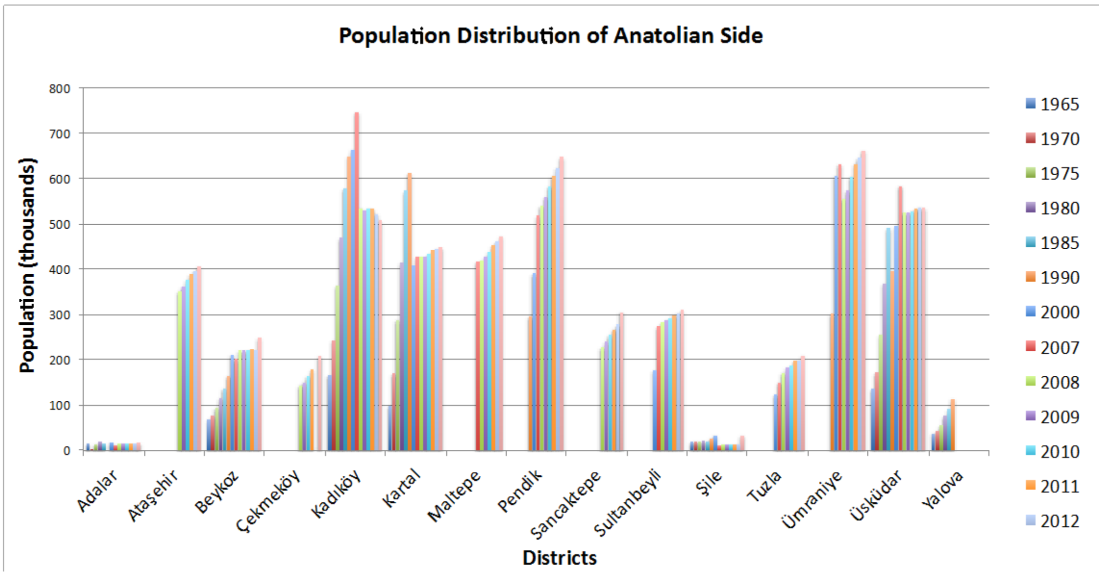

Figure 2.6 : Population change in Anatolian side of Istanbul between 1965 and 2013.

3. DATA

3.1 Meteorological Observations

Turkish State Meteorological Service (TSMS) which has established its first network around 1920s with a very basic network, then the network gradually spread country-wide, is mostly responsible for the coordination and maintenance of the meteorological observation network in Turkey. However, the significant expansion of the network in Turkey, has been started after 1960s. After 2007, conventional meteorological stations have been replaced gradually with the automatic weather stations. Within the last decade, some of the municipalities start to take meteorological observations along with the air quality observations to use in case of weather related events in the city. Additionally, Istanbul Disaster and Emergency Operation Directorate under İstanbul Municipality are established to coordinate mitigation and response efforts of the departments within the municipality in case of technological, anthropogenical and natural disasters. In order to notify the relevant departments of the municipality in case of extreme weather events that might affect the operations on the city, directorate began to form meteorological network.

In this study, meteorological data such as air temperature, relative humidity, wind speed and direction were provided from 6 TSMS (Turkish State Meteorology Service) stations which have observations starting from 1965, 3 TSMS automatic weather stations which have data after 2003, and 31 DCC (Disaster Coordination Center) observation network that start after 2007. Figure 3.1 illustrates the location of the meteorological stations in Istanbul. The stations represented by red and orange dots are TSMS stations (red ones are long term, orange ones are automatic stations) and the stations with yellow color belong to Disaster Coordination Center observation.

Figure 3.1 : **Locations of the meteorological stations in Istanbul.**

Table 3.1 lists the latitude, longitude, data period and missing number of data for each station. Red cells represent TSMS (long term) stations, green cells represent TSMS (automatic) stations and blue cells represent DCC stations. The observation interval of automatic stations is minute while the conventional station data interval is day. In the present study, the measurements are set up consisting of three urban (Kartal, Göztepe and Florya) and one suburban (Şile) station. Unfortunately, none of the meteorological stations within the Istanbul Municipality can be characterized as rural station.

Table 3.1 : Latitude, longitude, data period, missing number of data (days) and elevation (meters) for each meteorological station in Istanbul.

Station Name	Lat	Lon	Start	End	Missing Data	Elevation
Florya	40.97 N	28.78 E	01/01/60	31/10/13	229	37 m
Göztepe	40.98 N	29.05 E	01/01/60	31/10/13	239	41 m
Kartal	40.91 N	29.15 E	01/01/65	31/10/13	770	18 m
Kilyos	41.25 N	29.03 E	01/01/60	31/10/13	102	38 m
Sarıyer	41.14 N	29.05 E	01/01/60	31/10/13	101	59 m
Şile	41.16 N	29.60 E	01/01/60	31/10/13	202	83 m
Catalca Radar	41.34 N	28.35 E	13/03/03	30/10/12	635	381 m
İDBE	41.01 N	28.96 E	30/04/04	30/10/12	240	10 m
Samandira	40.98 N	29.21 E	30/04/04	30/10/12	60	123 m
AKOM	41.1 N	28.96 E	01/01/07	13/08/12	493	88 m

Table 3.2 (continued) : Latitude, longitude, data period, missing number of data (days) and elevation (meters) for each meteorological station in Istanbul.

Station Name	Lat	Lon	Start	End	Missing Data	Elevation
Aksaray	41.03 N	28.90 E	01/01/07	31/12/10	470	4 m
Alemdağ	42.04 N	29.27 E	12/12/07	13/08/12	22	175 m
Arnavutköy	41.17 N	28.75 E	21/11/07	13/08/12	16	170 m
Ataşehir	41.00 N	29.10 E	20/11/07	13/08/12	56	60 m
AHL-Bakirköy	40.99 N	28.81 E	29/11/07	13/08/12	47	12 m
Beşiktaş-Yıldız	41.05 N	29.00 E	19/11/07	13/08/12	24	93 m
Beylikdüzü	41.00 N	28.67 E	19/11/07	13/08/12	396	55 m
Büyükçekmece	41.02 N	28.61 E	12/12/07	13/08/12	6	155 m
Çamlica-Libadiye	41.02 N	29.07 E	12/11/07	13/08/12	98	150 m
Çanta	41.1 N	28.08 E	01/01/07	13/08/12	550	116 m
Çavuşbaşı	41.08 N	29.15 E	01/01/07	13/08/12	431	137 m
Esenler	41.04 N	28.89 E	19/11/07	13/08/12	163	85 m
GOP	41.09 N	28.92 E	30/11/07	30/12/10	286	46 m
Haıimköy	41.05 N	28.63 E	01/01/07	13/08/12	835	183 m
Haliç	41.04 N	28.94 E	05/02/08	13/08/12	63	25 m
İstoç-M.Bey	41.06 N	28.84 E	11/12/07	13/08/12	291	90 m
Kamiloba	41.05 N	28.43 E	01/01/07	13/08/12	504	54 m
Kartal-U.Mumcu	40.94 N	29.21 E	27/11/07	13/08/12	149	195 m
Kınalı	41.12 N	28.16 E	12/12/07	13/08/12	437	28 m
Maslak-İTÜ	41.09 N	29.02 E	12/12/07	13/08/12	38	76 m
Olimpiyat	41.1 N	28.76 E	01/01/07	13/08/12	496	100 m
Ömerli	41.00 N	29.33 E	01/01/07	12/08/12	551	153 m
Pendik	40.88 N	29.23 E	12/12/07	30/12/10	32	45 m
Selimpaşa-Kav.	41.10 N	28.33 E	15/01/08	13/08/12	27	91 m
Şile	41.16 N	29.50 E	09/11/07	13/08/12	128	128
Terkos	41.31 N	28.66 E	01/01/07	13/08/12	514	4 m
Tuzla-Bayram.	40.87 N	29.38 E	28/11/07	13/08/12	22	135 m
Ümraniye	41.03 N	29.12 E	14/11/07	13/08/12	32	135 m
Zekeriyaköy	31.19 N	29.00 E	12/12/07	12/08/12	16	225 m
Zincirlikuyu	41.06 N	29.01 E	19/11/07	13/08/12	187	127 m

3.2 Land Use Data

To generate the land use distribution for Istanbul, three different datasets are used:

- Geographical data of the Istanbul Metropolitan Municipality,
- Basar Soft GIS (Geographic Information System) Data and
- CORINE (Coordination of Information on the Environment) Land Cover Raster Data

For this study, land use data provided by Geographical data of the Istanbul Metropolitan Municipality and Basar Soft GIS (Geographic Information System) Data has been chiefly used for classification of buildings because of their good resolution and availability. CORINE Land Cover Data fills the spaces where the Geographical data of the Istanbul Metropolitan Municipality and Basar Soft GIS, provides no data, especially for the vegetation cover and green areas. The land use classes used in Municipality dataset are more similar to the classes that Basar Soft GIS Data used in comparison with the Corine dataset. Thus, it was more easy to integrate them into the land use classes created in this work.

4. MUKLIMO_3 (MICRO-SCALE URBAN CLIMATE MODEL)

4.1 Description of a Model

In this thesis, the thermodynamic version of the micro-scale urban climate model MUKLIMO_3 developed by the DWD (German Meteorological Service – Deutscher Wetterdienst) is used to simulate the urban climate and planning applications of Istanbul. In order to scale down further the regional climate projections to urban scale, empowering a simulation of a city and its surroundings, MUKLIMO_3 (Sievers 1995) is employed on the urban scale. The non-hydrostatic thermodynamic version of MUKLIMO_3 simulates the atmospheric temperature, humidity and wind field on a three-dimensional model grid. For this purpose, the basic model MUKLIMO, which solves Navier-Stokes equations to simulate the atmospheric flow fields, was generalized with the streamfunction–vorticity method to three dimensions (Sievers 1995). The model is enhanced with prognostic equations for atmospheric temperature and humidity, balanced heat and moisture budgets in the soil (Sievers et al. 1983) and a sophisticated vegetation model (Siebert et al. 1992). The numerical approach for the calculation of short-wave irradiances at the ground level, the walls and the roof of buildings in an environment with unresolved built-up is described by Sievers and Früh (2012). A simple formulation for turbulent mixing with the first-order closure of the turbulence scheme based on the Monin-Obukhov similarity theory (MOST) and the Prandtl mixing length approach (Sievers, 1987; 2012) is used by MUKLIMO_3. Above the lowest atmospheric level, the model uses the Blackadar's mixing length (l_∞=30 m for neutral and stable conditions) which is adapted according to the stability criteria. The height of the convective layer calculated within the time-varying 1D model is used to calculate the mixing length for unstable conditions. In addition, the mixing length is modified in presence of buildings and trees. The model takes into account the effects of cloud cover on radiation. However, it does not include cloud processes, precipitation, horizontal runoff or anthropogenic heat.

Gross (1989) already indicated that the flow between buildings is parameterized through a porous media approach for unresolved buildings. Maximum of 99 different land use classes can be defined including specific land surface characteristics listed in a land use table. In general, the values are derived from geographical (GIS) data, which are provided by local and federal government or GIS companies. Land use types are classified as four main categories: built-up areas, traffic, vegetation and water bodies. For each land use class, a set of parameters is identified to describe land use features and urban structures in the land use table: for instance fraction of built-up area (γ_b), mean building height (h_b), wall area index (w_b), fraction of pavement of the non-built area (v), fraction of tree cover (σ_t) and fraction of low vegetation of the remaining surface (σ_c), height (h_c) and leaf area index (LAI_c) of the canopy layer as well as mean height (h_t) and leaf area index (LAI_t) of the trees. The vegetation is divided into 3 vertical layers: tree crown, tree trunk and low vegetation.

The thermodynamic version of MUKLIMO_3 simulates a limited area of the atmosphere therefore the model requires initial and boundary conditions. From a given set of initial variables (from 1 to 5 corresponding values per height level): relative humidity (rh), air temperature (T), and horizontal wind vector (y) characterizing the environmental conditions the model first computes a one-dimensional profile up to 1100-m altitude, in order words; 1D model version of MUKLIMO_3 is used in order to initialize the 3D simulation. The profile description also involves wind direction, reference height, soil temperature, indoor temperature and water temperature but these variables are not specified by more than one value. This one-dimensional profile performs the meteorological conditions with effect from topography and land use cover. During the three-dimensional integration process, the top of the three-dimensional domain interchanges from one-dimensional profile values at 750 m altitude and takes as time-dependent upper boundary values (Früh et al. 2011). Initially, moisture and soil temperature are specified constant throughout the soil column. The values for air temperature, relative humidity and wind are used to initiate the 3D model run consider terrain height and soil type, after running the 1D model for a day. The first hour of the 3D model simulation, is excluded from the analysis. The 1D model continues to supply upper boundary conditions for the whole duration of the 3D model simulation.

Typical integration times for MUKLIMO_3 reach from several hours up to days. The horizontal and vertical resolution of the model varies with application (simulation of the resolved built-up or unresolved built-up environment). For unresolved built-up the horizontal resolution of the model is typically between 20 m and 500 m where the horizontal resolution in this study is 200 m. Figure 4.1 shows the MUKLIMO_3 modeling system based on the current source code, released in October 2013, and two further Fortran90 tools for post-processing procedures.

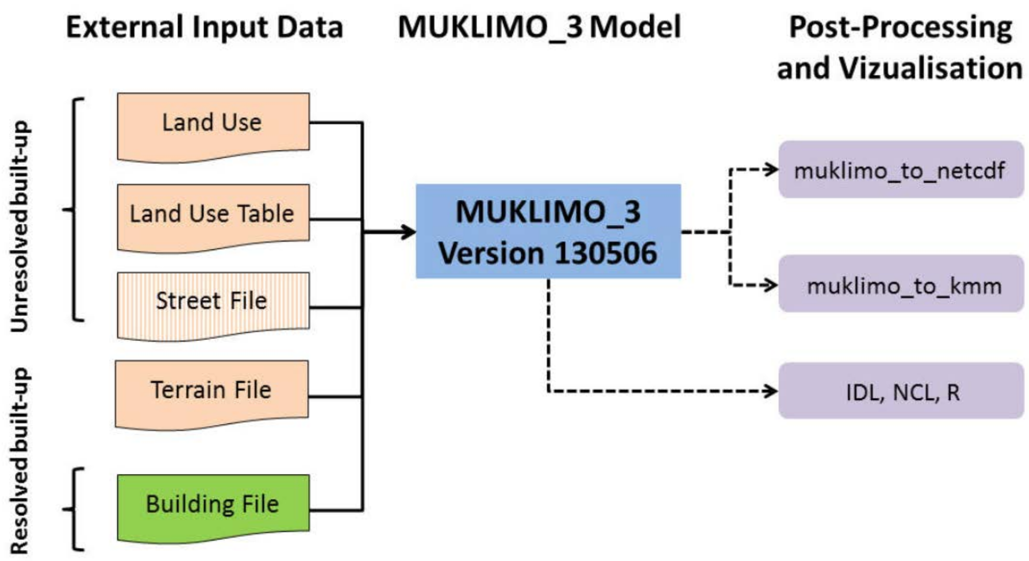

Figure 4.1 : MUKLIMO_3 modeling system.

Sensitivity simulations are started on 02 August 2014 besides mitigation simulations are started on 07 August 2012 with 1 hour spin up for the 1D boundary model. Climatological records support that most summer days occur between June to August and generally July 15 is chosen as a representative day since this day has an average sun height and day length for the conditions in June to August. However, for Turkey especially for Istanbul, the strongest summer days are occured on August therefore the time period of both sensitivity analysis and mitigation strategies simulations are performed for selected days in August.

The atmospheric conditions of August 2nd represents a typical summer day of Istanbul. Therefore, this date is selected to force MUKLIMO_3 for sensitivity analysis. The 3D simulations are started on 02 August 2014 at 10 am CEST (Central European Summer Time) and ended on 03 August 2014 at 9 am CEST for the sensitivity analysis and 07 August 2012 at 10 am CEST (Central European Summer Time) and ended on 08 August 2012 at 9 am CEST for the mitigation strategies.

Only the time period between 10 am CEST till 9 am CEST for the next day is evaluated, the first and the last hours of the simulations are ignored for the model stability. Moreover, the mitigation stratigies have been performed for a day under heat wave effect for Istanbul.

4.2 Equations of the Model

4.2.1 Prognostic equations

The equation of motion is used in Boussinesq approximation (Sievers and Zdunkowski, 1986), i.e.,

$$\frac{\partial \vec{v}}{\partial t} + \vec{v} \cdot \nabla \vec{v} + \frac{1}{\rho_o} \nabla \mathrm{p} = \vec{g}\left(1 - \frac{\theta'}{\theta_o}\right) - \frac{1}{\rho_o} \nabla \cdot \vec{j} - f\vec{k} \times \vec{v} \tag{4.1}$$

where ρ_o and θ_o represent constant mean values of the density and the potential temperature, and θ' is the deviation of θ from θ_o, $\vec{g}$ is a three dimensional constant, $\vec{j}$ is stress tensor and the $\vec{v}$ represent stream velocity. The equation (4.1) makes use of the anelastic approximation implying "density fluctuations are caused by temperature fluctuations only. Pankart (1975) uses essentially the same equation but neglects the Coriolis effect. The incompressibility condition that is given with equation (4.2);

$$\nabla \cdot \vec{v} = 0 \tag{4.2}$$

must always be satisfied. The stress tensor $\vec{j}$, which is explained by equation (4.3), is parametrized by means of a gradient law,

$$\vec{j} = -\rho_o K_m \left(\nabla \vec{v} + \vec{v} \nabla\right) \tag{4.3}$$

where K_m is the tur. exchange coefficient for momentum.

The energy budget of the atmospheric system. is described by heat equation (4.4),

$$\frac{\partial}{\partial t}\theta + \vec{v} \cdot \nabla\theta + \frac{1}{\rho_o c_p} \nabla \cdot \vec{j}^q = \frac{1}{\rho_o c_p} Q \tag{4.4}$$

where the source Q, representing anthropogenic heat production, is a given function of position and time. The turbulent heat flux j^q is expressed as equation (4.5):

$$\vec{j}^q = -\rho_o c_p K_h \nabla\theta \tag{4.5}$$

The exchange coefficient for heat K_h is also used for the exchange of matter.

The third prognostic equation of the model is the transport equation (4.6) given by

$$\frac{\partial c}{\partial t} + \vec{v} \cdot \nabla c + \frac{1}{\rho_o} \nabla \cdot \vec{j}^c = \frac{1}{\rho_o} Q^c \tag{4.6}$$

Where c represents an arbitrary mass concentration. This equation is applied for pollutants, e.g., carbon monoxide and for the atmospheric moisture. The quantity Q^c is a volume source of c, and the diffusion flux j^c is parametrized as equation (4.7):

$$\vec{j}^c = -\rho_o K_h \nabla c \tag{4.7}$$

4.2.2 Stream function-vorticity method

MUKLIMO_3 is predicated the work of Sievers and Zdunkowski (1986) on the stationary wind field in a neutral layered atmosphere called the stream function-vorticity method and the model derive this method for three dimensions. The main point is to predict the two-dimensional vorticity field, instead of combining the Navier-Stokes equation. This method has several advantages. On the one hand, the filter condition of being divergence free is performed, which is required for micro-scale simulations and avoids acoustic waves. Also, there is only one vector equation with one condition left to solve.

Just like the equation of motion, the stream-vorticity function is used in Boussinesq Approximation equation (4.8):

$$\frac{\partial \vec{v}}{\partial t} + \vec{v} \cdot \vec{\nabla} \vec{v} + \frac{1}{\rho_o} \vec{\nabla} \vec{p} = \vec{g} \left(1 - \frac{\rho'}{\rho_o}\right) - \frac{1}{\rho_o} \vec{\nabla} \cdot \vec{J} - 2\vec{\Omega} \times \vec{v} \tag{4.8}$$

where $\rho_o + \rho' = \rho$ represent density, $\overline{\Omega}$ is angular velocity of the earth and all other parameters are explained in the previous part 4.2.1. According to the incompressibility condition, the divergence has to be zero again showing by equation (4.9):

$$\vec{\nabla} \cdot \vec{v} = 0 \tag{4.9}$$

It is well known that this can be satisfied by expressing $\bar{v}$ as equation (4.10):

$$\vec{v} = -\vec{\nabla} \times \overline{\Psi} \tag{4.10}$$

where $\overline{\Psi}$ is a vector potential or vector stream function. Actually, this vector potential is not individually determined but there exists the possibility of gauge transformations $\vec{\Psi} \rightarrow \vec{\Psi} + \vec{\nabla}\lambda$ with arbitrary scalar functions λ. These tranformations leave the velocity field $\bar{v}$ unchanged. The stream function $\overline{\Psi}$ is related to the vectorial vorticity $\xi = \nabla \times \vec{v}$.

In order specify the stream-function method the main steps are investigated for two dimensions to simplify matters.

The common solution of the Navier-Stokes equation is integration to get the wind field. The main force of the wind field (∇p) was not yet known but Sievers (1995) solved this significant problem by converting them to the vorticity coordinate system.

$$(u, w) \rightarrow \xi = \frac{\partial u}{\partial z} - \frac{\partial w}{\partial x} \tag{4.11}$$

Then, retransformation can be done with the help of stream-function approach, which is shown by equation (4.12), (Sievers, 1995):

$$u = \frac{\partial \psi}{\partial z}, w = -\frac{\partial \psi}{\partial x} \tag{4.12}$$

with the definition of the stream function $\vec{\nabla}^2 \vec{\psi} = \xi$.

In three dimensions, there are two equations for ξ (ξ_1 and ξ_2) due to one additional dimension. Combining all the equations and eliminating the vertical velocity by the help of the incompressibility condition a pair of two partial differential equations called the stream-function equations (equation (4.13) and equation (4.14)) can be derived (Sievers, 2012).

$$\xi_1 = \frac{\partial^2 \psi_1}{\partial y^2} + \frac{\partial^2 \psi_1}{\partial z^2} - \frac{\partial^2 \psi_2}{\partial y \partial x} \tag{4.13}$$

$$\xi_2 = \frac{\partial^2 \psi_2}{\partial x^2} + \frac{\partial^2 \psi_2}{\partial z^2} - \frac{\partial^2 \psi_1}{\partial x \partial y} \tag{4.14}$$

By differentiation of ξ_1, the wind field equation (4.15) can be diagnosed:

$$u = \frac{\partial \psi_2}{\partial z}, v = -\frac{\partial \psi_1}{\partial z}, w = \frac{\partial \psi_1}{\partial y} - \frac{\partial \psi_2}{\partial x} \tag{4.15}$$

Based on this method, MUKLIMO_3 simulates the wind field in urban areas depending on the elevation of the buildings developed in the simulation area and the prevailing wind direction and velocity of the whole simulation area.

4.2.3 Exchange coefficient

The exchange coefficients for momentum K_m and for heat and matter K_h are modeled by means of a mixing length formula. For simplicity no difference is made between K_m and K_h, i.e., $K_m = K_h = K$.

The equation (4.16) is given by

$$K = l^2 |\nabla \times \vec{v}| \Phi(Ri) \tag{4.16}$$

where l is the mixing length and $\Phi(Ri)$ a function describing the stability dependence of K. The Richardson Number Ri is defined as equation (4.17):

$$Ri = -\frac{g \cdot \nabla\theta}{\theta |\nabla \times \vec{v}|^2} \tag{4.17}$$

The previous equations are obtained from commonly used expressions by the replacement,

$$\frac{\partial v_h}{\partial z} \rightarrow |\nabla \times \vec{v}| \tag{4.18}$$

which equation (4.18) has the purpose to make K invariant against rotations of the velocity field.

Following Blackdar (1962), the mixing length is modeled as equation (4.19)

$$l = l(\vec{x}) = \frac{K\{d(\vec{x}, G) + z_o\}}{1 + \frac{K\{d(\vec{x}, G) + z_o\}}{\lambda_{BL}}} \tag{4.19}$$

Where d(x,G) is the minimum distance between the position x and the lower boundary G. The length λ_{BL} which is an upper limit of l is considered an external parameter of the model and chosen with respect to equation (4.20);

$$\lambda_{BL} = \begin{cases} 100\ m\ for\ unstable\ stratification \\ 30\ m\ for\ neutral\ conditions \\ 12.5\ m\ for\ stable\ stratfication \end{cases} \tag{4.20}$$

according to Wu (1965). The stability function $\Phi(Ri)$ is specified as equation (4.21);

$$\Phi(Ri) = \begin{cases} \sqrt{1\text{-}\alpha Ri} & for\ Ri \leq 0 \\ \sqrt{1 - \dfrac{\alpha Ri}{1 + \alpha Ri}} & for\ Ri > 0 \end{cases} \quad with\ \alpha = \epsilon \tag{4.21}$$

This formulation assures that the exchange coefficient remains real and finite in both limits Ri → ±∞. To first order in Ri it is in accordance with Gutman and Toorance (1975).

4.3 Creating Land Use Cover

The urbanization negatively impacts the heat stress of urban areas. So that it is important to investigate what type of changes in the urban landscape affect the near-surface climate and elevate the intensity of UHI in the city. The relationship between urbanization and long-term modification of the urban climate of Istanbul is investigated by modeling the present-day spatial distribution of the urban heat load.

In order to simulate the urban climate with MUKLIMO_3 or other urban climate models, some information about the structure, elevation and the material of the city, such as the distribution, height and fraction of buildings, height of the canopy layer, leaf area index of trees, etc. are needed. Then, these information has to be translated into a specific (ASCII) format that the model can process.

The essential part of creating land use cover and run the model is to determine appropriate land use classes (shown in Figure 4.2), which can perform complex terrain of Istanbul properly, and each of them are identified with 24 different physical parameters in the land use table.

Typ	Land Use Class Name
1	Type 1.1 Building (5-15% Density & <10 m Height)
2	Type 1.2 Building (5-15% Density & 10-20 m Height)
3	Type 1.3 Building (5-15% Density & 20-30 m Height)
4	Type 1.4 Building (5-15% Density & >30 m Height)
5	Type 2.1 Building (15-30% Density & <10 m Height)
6	Type 2.2 Building (15-30% Density & 10-20 m Height)
7	Type 2.3 Building (15-30% Density & 20-30 m Height)
8	Type 2.4 Building (15-30% Density & >30 m Height)
9	Type 3.1 Building (30-50% Density & <10 m Height)
10	Type 3.2 Building (30-50% Density & 10-20 m Height)
11	Type 3.3 Building (30-50% Density & 20-30 m Height)
12	Type 3.4 Building (30-50% Density & >30 m Height)
13	Type 4.1 Building (>50% Density & <10 m Height)
14	Type 4.2 Building (>50% Density & 10-20 m Height)
15	Type 4.3 Building (>50% Density & 20-30 m Height)
16	Type 4.4 Building (>50% Density & >30 m Height)
17	traffic & parking area
18	bare soil
19	Coniferous forest
20	Broad-leaved forest
21	Mixed forest
22	agriculture
23	wasteland with grassland and shrubbery
24	wasteland with grassland
25	water

Figure 4.2 : Land use classes that are prepared for Istanbul.

The new urban land use types are defined by considering the spatial coverage and the average height of the buildings. The spatial distribution of the land uses, which is used to simulate the urban climate of Istanbul in this work, is shown in Figure 4.3. In this figure the city borders of Istanbul are represented by the 551x361 grid boxes and the horizontal resolution of each cell is 200 meter.

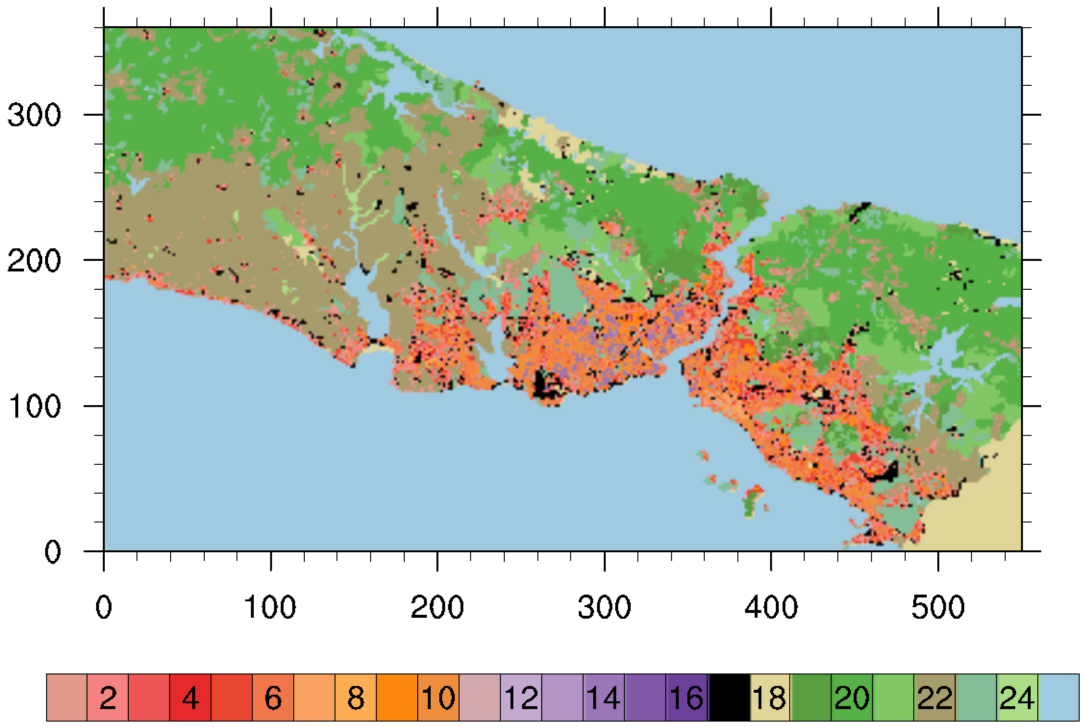

Figure 4.3 : The spatial distribution of land use classes for Istanbul.

Combining the three land use datasets, which all together have about more than 100 land use classes, similar land use types have been combined, too, because it is not necessary to define each existing land use class. The final land use classification, which is specified as 25 classes, used to simulate the urban climate of Istanbul with MUKLIMO_3 can be seen in Figure 4.2.

The first group of land use classes (up to No. 16) are residential areas with different densities and heights; The land use types 1, 2, 3 and 4 represent low density built-up area which covers the 5%-15% of a grid, with low buildings which are less then 10 m height (1), medium's which have a height between 10 to 20 meters (2), high's are from 20 to 30 m height (3) and very high (4) which are above the 30 meters height. The types of 5, 6, 7 and 8 show medium dense residential area take space from 15% to 30% per a grid area with low (5), medium (6), high (7) and very high (8) height characteristics and the classes of 9, 10, 11 and 12 indicate the dense built-up area that is covered by the range of 30%-50% area in a grid with low (9), medium (10), high (11) and very high (12) height. The high density residential area which encompass the area more than 50% per grid is summarized by the type numbers of 13, 14, 15 and 16, depending on the height of the buildings by terms of low (13), medium (14), high's (15) and very high (16) ones.

The class of (17) shows the traffic and parking area, while the last section of land use classes represents green and open areas (from 18 to 24, highlighted in hue of green) without any buildings, but eventually with trees, grass or wasteland. The following land uses describe bare soil (18), from 19 to 22 represent forested area with different types of leaf; coniferous forest (19), broad leaf forest (20) and mixed forest, (22) performs agricultural area, the classes 23 and 24 show the wastelands with shrubbery and grassland, respectively. The land use type water is represented by (25).

In order to create valid classes for residential areas, the density percentage of each land use classes in a single grid which has a 200 m x 200 m area are investigated. Some of the grids are fully represented by a single land use type, whereas some of them can not be shown without more than one class type. The MUKLIMO modeling system can not allow to identify two different land use type in a single grid, that is why using just one class per grid is needed. For instance, if a density percentage of a medium dense built-up area with low height buildings (5) cover 50% of a grid area, the density percentage of a low density residential area with high buildings (3) is 30% and broad leaf forested area (20) is about 20%; then the greater part of a grid is composed of a land use type (5) which is medium dense residential area, so the grid should be represented by this type number rather than (3) or (20). All these classifications belong to built-up area are compilation of geographical data of the Istanbul Metropolitan Municipality and Basar Soft GIS and are made by the assumption that is explained below. With the exception of residential area's classification, the rest of the land uses (parking & traffic area, green areas and water) have been adopted from the land use classes provided by CORINE Land Cover. The grids of CORINE Data are converted into the same grid size (200 m x 200 m) that is used in this study by using of ArcGIS which is a geographic information system for working with maps and geographic information.

4.4 Definition and Modification of the Land Use Table

In order to describe each land use with physical information about the buildings, the green areas, the water bodies and the free land, the land use table for MUKLIMO called LUTAB summarizes all the information about the landuse classes, for instance, the leaf area index of the canopy layer, the building fraction, the height of the buildings, the surface roughness, etc. Both types are connected by the number belonging to each class, which can also be seen in Table 4.2.

Each of the land use classes are identified with 24 different physical parameters in the land use table. These physical parameters that describe the land use classes are determined by model developers in Germany, but not totally suitable for the mega city Istanbul which is why some of the parameters such as leaf area index (LAI), height of the building, etc. were modified into conditions of Istanbul. All the physical parameters required by MUKLIMO3 are described in Table 4.1.

Table 4.1: Description of the physical parameters required by MUKLIMO3 to simulate the urban climate. All values are mean values, which represent each landuse class in the whole simulation area.

Parameters	Description
Typ	Identification number
vg1/vg2	Building fraction of the first/second building typ
wai1/wai2	Wall area index of the first/sencond building typ
h1/h2	Mean building height of the first/second building typ
vs	Fraction of impervious surface between buildings
z0	Surface roughness of the non built-up areas in meter
hbm	Tree height in m
hst	Stem height in m
bf0	Leaf area densitiy in the stem area in m^{-1}
bf1	Leaf area densitiy in the tree top area in m^{-1}
lai	Leaf area index of the canopy layer, dimensionless
hca	Vegetation height of the canopy layer in m
sigbm	Tree cover (amount of trees), dimensionless
sigma	Vegetation cover of the canopy layer, dimensionless
grant	Fraction of green roof
albw	Albedo of the walls
albd	Albedo of the roofs
albvs	Albedo of the impervious parts of the canopy layer
kwand	K-value of the building walls in $W/(m^2*K)$
kdach	K-value of the building roofs in $W/(m^2*K)$
cwand	Area heat capacity of the building walls in $J/(K*m^2)$
cdach	Area heat capacity of the building roofs in $J/(K*m^2)$

The first group of parameters describes the land use type of buildings. The building fraction of the first, second building type in one gridbox (*vg1*, *vg2*), the mean wall area index of the first, second building type (*wai1*, *wai2*) and the height (*h1*, *h2*) of the first, second building type has to be defined. Thus, it is possible to define two types of buildings, which is helpful if there are small and large buildings in one landuse class for instance number "4" *(vg1=0.1, h1=54 and vg2=0.3, h2=33.5)* and "8" *(vg1=0.22, h1=50 and vg2=0.4, h2=33.5)* in the LUTAB represent two different types of building in the same grid. In this study, the information about the height of the buildings (*h*) and the percentage of buildings *(vg)* has been provided from Basar Soft GIS Data, the wall area index (*wai*) has been calculated from geographical data of the Istanbul Metropolitan Municipality. The fraction impervious surface in other words sealing (*vs*) is related to no-built-up areas between buildings or trees, and has been estimated proportionally to the fraction of the built-up area therefore, the more percentage of buildings correspond the more sealing area. The surface roughness of the non built-up areas or areas below trees in meter (z_0) refers to this area between the buildings, too, and thus does not have great differences between the default LUTAB which was generated by DWD especially for the classes related with the built-up area. However, the roughness length for the classes which represents the non built-up areas (green areas, wasteland, traffic and parking areas, etc.) are not totally suitable for the mega city Istanbul hence some modification has been made, for instance the roughness length of the forested area is determined by model developers in Germany as 0.2 meter, but this values has been changed to 0.4 meter by the help of the surface characteristics of Istanbul. The next group of parameters refers to non built-up areas between the buildings (greenery area, traffic area, wasteland and water body). Information about the forested area is also described, but they only have an effect if percentage of the first building type (*vg1)* and percentage of the second building type (*vg2)* are not used. Due to the fact that built-up and non built-up area cannot be in the same landuse class, one has to decide whether trees or buildings are dominant. Some of the parameters for the canopy layer have been adapted from the default LUTAB of DWD, but the majority of these parameters has been estimated by the help of some documentation about the tree structure of Istanbul.

Table 4.2 : Definition of the parameters from Table 4.1 to define the landuse classes.

Typ2	vg1	vg2	wai1	wai2	h1	h2	vs	z0	hbm	hst	bf0	bf1	lai	hca	sigbm	sigma
1	0.10	0	2,0	0,0	7.5	0,0	0.1	0.20	0.00	0	0	0	1	1	0	1,0
2	0.10	0	2.5	0,0	13,0	0,0	0.1	0.2	0	0	0	0	1	1	0	1,0
3	0.10	0	4.5	0,0	24,0	0,0	0.2	0.2	0	0	0	0	1	1	0	0.9
4	0.10	0.3	9,0	6,0	54.5	34,0	0.2	0.2	0	0	0	0	1	1	0	0.9
5	0.22	0	2,0	0,0	8,0	0,0	0.3	0.21	0	0	0	0	1	0.7	0	0.8
6	0.22	0	2.5	0,0	13,0	0,0	0.3	0.2	0	0	0	0	1	0.7	0	0.8
7	0.22	0	4.5	0,0	23.5	0,0	0.4	0.2	0	0	0	0	1	0.7	0	0.7
8	0.22	0.4	5,0	5,0	50,0	33.5	0.4	0.2	0	0	0	0	1	0.7	0	0.7
9	0.45	0	1.5	0,0	8.5	0,0	0.5	0.22	0	0	0	0	1	0.5	0	0.6
10	0.45	0	2,0	0,0	13.5	0,0	0.5	0.2	0	0	0	0	1	0.5	0	0.6
11	0.45	0	3.5	0,0	22,0	0,0	0.6	0.2	0	0	0	0	1	0.5	0	0.5
12	0.40	0	2.5	0,0	40.5	0,0	0.6	0.2	0	0	0	0	1	0.5	0	0.5
13	0.60	0	0.5	0,0	8.5	0,0	0.7	0.23	0	0	0	0	1	0.3	0	0.4
14	0.60	0	1,0	0,0	14.5	0,0	0.7	0.2	0	0	0	0	1	0.3	0	0.4
15	06.0	0	1.5	0,0	22.5	0,0	0.7	0.2	0	0	0	0	1	0.3	0	0.3
16	0.50	0	1.5	0,0	49.5	0,0	0.7	0.2	0	0	0	0	1	0.3	0	0.3
17	0	0	0	0	0	0	0.50	0.3	8,0	2,0	0.1	0.3	1.5	0.50	0.20	0.20
18	0	0	0	0	0	0	0.05	0.1	0	0	0	0	1,0	0.20	0.00	0.20
19	0	0	0	0	0	0	0,0	0.4	10,0	4,0	0.2	0.3	2,0	0.50	0.6	0.5
20	0	0	0	0	0	0	0,0	0.4	10,0	4,0	0.2	0.3	3,0	0.50	0.6	0.5
21	0	0	0	0	0	0	0,0	0.4	10,0	4,0	0.2	0.3	2.5	0.50	0.6	0.5
23	0	0	0	0	0	0	0.05	0.20	0.00	0.00	0,0	0,0	1,0	1.00	0.00	0.90
24	0	0	0	0	0	0	0.20	0.1	0.00	0.00	0,0	0,0	1,0	0.30	0.00	0.5
25	0	0	0	0	0	0	1.00	0.05	0.00	0.00	0,0	0,0	0,0	0.00	0.00	0.00

The characterictic of the trees is well defined in the default land use table which were generated for Germany and not similar for the tree structure of Turkey since the distinctive climate conditions, elevation and location. Therefore, the parameters for leaf area index, height of the trees, etc. need to be modified in order to improve the representation of land use for Istanbul. For example, the tree height was 20 meter for the land use class of forest in the default LUTAB however, this value does not represent the forested area of Istanbul well. Thus, the tree height has been changed into 10 m from 20 m by using the sources of the ministry of forestry and water affairs.

Accordingly, while changing the tree height, the leaf area index has also been modified. In the default LUTAB, the leaf area index was 0.5 for the land use class forest, but in this study, as the forested area is divided into 3 categories such as coniferous forest, broad-leaf forest and mixed forest; the leaf area index of each of these forest types has been reestimated with reference to the study about the sensitivity of BATS land surface parametrization scheme (Handerson-Sellers, 1992) and determined as 0.2, 0.3 and 0.25 respectively.

In the default land use table (LUTAB), some values such as fraction of green roofs, albedo of the walls/roofs, heat capacity of the building walls/roofs, etc. are not specified, but they are filled with standard values which are embedded in the MUKLIMO Fortran code. In order to test and improve the effectiveness of these parameters, mitigation strategies have been performed and the anomaly between reference simulation and scenerios has been calculated in this study.

The final LUTAB for the reference simulation of this study can be seen in Table 4.2.

5. ANALYSIS AND RESULTS

5.1 Urban Heat Island

City centers are generally warmer than their surrounding areas (Oke, 1982). In urban areas, human-induced local climate conditions and high nocturnal temperatures caused by heat absorption in pavement and concrete surfaces due to the reduced evaporative cooling is defined as urban heat island effect. This is one of the most significant phenomenon of the 21st century and this phenomenon is effected by several parameters, for instance the lack of vegetation contributes to the formation of urban heat islands and hence intensive built-up areas have relatively higher nocturnal temperatures than surrounding rural or agricultural areas due to the absorbed solar energy and produced thermal energy by the modified land surfaces. The surface and air temperature distribution over rural, urban and suburban areas is shown at Figure 5.1.

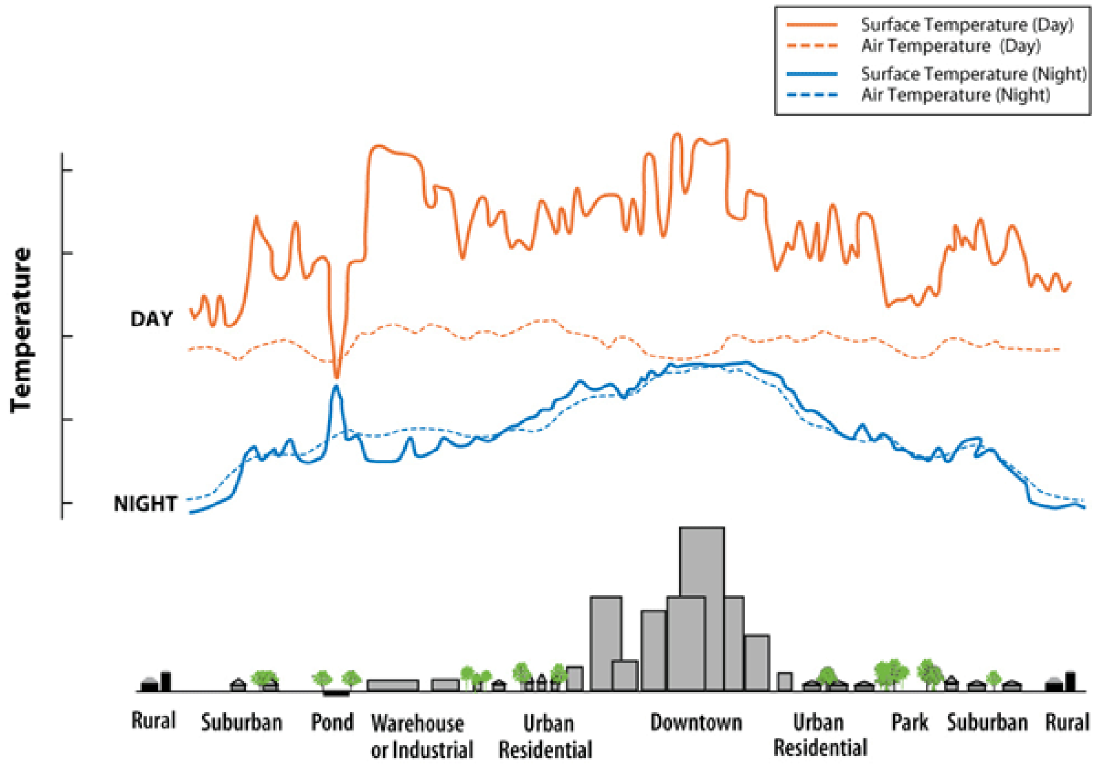

Figure 5.1 : The surface and air temperature distribution over rural, urban and suburban areas.

The minimum temperature differences between the urban and the rural area determines the urban heat island effect of a city and is called urban heat island intensity (UHII) (Oke, 1987):

$$UHII = T_{urban} - T_{rural}$$

In general, the urban heat island effect can be described by the changed energy balance in the city, which was first described by Oke (1982):

$$Q^{*} + Q_F = Q_E + Q_H + Q_S$$

with Q^{*} : surface net radiant flux density, Q_F : anthropogenic heat flux, Q_E : sensible heat flux, Q_H : latent heat flux, Q_S : heat storage/release

In the present study, the measurements are set up consisting of four urban and two suburban stations. Unfortunately, none of the meteorological stations within the Istanbul Municipality can be characterized as rural station. Since the population of Şile located at the north coast of the city is under 20,000 inhabitants and hence it might be considered as suburban station. Kilyos station is located northern part of Sarıyer province and the land cover has usually green landscape. Therefore, Kilyos might be characterized as suburban station as well. The other four stations; Sarıyer, Göztepe, Florya and Kartal are categorized as urban stations. The UHI intensity is examined between the city center station and the suburban station explained above for daily maximum and daily minimum temperatures.

Table 5.1 : The seasonal UHI intensities based on Tmin and Tmax differences for urban and suburban stations.

Seasons	Tmin			Tmax		
	G.tepe-Şile	Kartal-Şile	Florya-Şile	G.tepe-Şile	Kartal-Şile	Florya-Şile
Spring	0.97	1.89	0.91	1.47	1.81	0.90
Summer	1.02	2.15	1.09	2.39	3.01	2.14
Fall	0.51	1.83	0.85	1.05	1.41	0.76
Winter	0.76	1.52	0.63	0.13	0.50	0.25

In order to estimate the strength of urban heat island in this mega city, daily maximum and minimum temperatures differences between urban and suburban stations are used. The seasonal UHI intensities based on T_{min} and T_{max} differences for urban (Göztepe, Kartal, Sarıyer and Florya) and suburban (Şile) stations are summarized in Table 5.1 and the location of these stations are shown in Figure 5.2. The red dots represent urban stations and the orange dot represents suburban station for this study**.** The UHI intensity is stronger during summer seasons and Kartal experiences intensified urban heat island effect more than the other urban areas. UHI intensities has been the found the maximum in summer for the all urban-suburban differences at each cases of T_{min} and T_{max}. The daytime (nighttime) UHI intensity defined with respect to Sile (suburban) varies between 0.41K and 3.01K (1.02K and 2.18K). During summer period, the UHI takes its maximum intensity between Kartal (urban) and Şile (suburban) sites of the city.

Figure 5.2 : The location of urban (red dots) and suburban stations (orange).

Figure 5.3, illustrates that the daytime and the nighttime urban heat island intensity over 6 TSMS (Turkish State Meteorology Service) long period stations, TSMS automatic weather stations and 31 DCC (Disaster Coordination Center) stations.

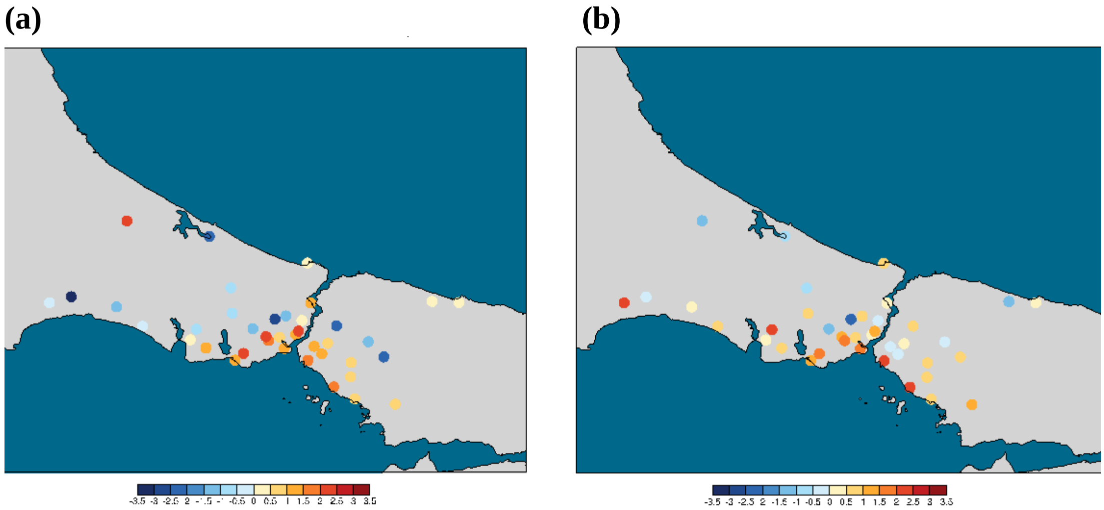

Figure 5.3 : The daytime (**a**) and the nighttime (**b**) UHI intensity over Istanbul.

The atmospheric UHI usually reaches its highest intensity on summer nights, and under calm air and a cloudless sky. Therefore, the total of 127 dry days, which have cloudiness less than 2/8 and wind speed less than 2 m/s are selected to estimate the strength of UHI in Istanbul. The daytime (maximum) and the nighttime (minimum) temperature differences under clear and calm atmosphere conditions are shown at Figure 5.4.

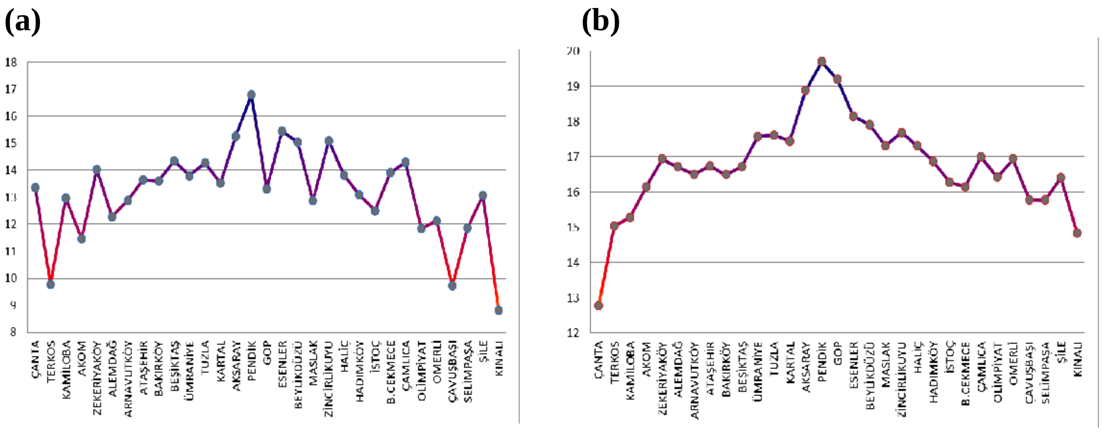

Figure 5.4 : The daytime **(a)** and the nighttime **(b)** temperature differences under clear and calm atmosphere conditions.

In Figure 5.5, the location of selected urban station (Pendik) and a rural station (Terkos), and in Figure 5.6, the land use distribution of these stations are shown.

Figure 5.5 : The location of a urban station Pendik (red dot) and a rural station Terkos (orange dot).

Figure 5.6 : The land use distribution of a urban station Pendik (red dot) and a rural station Terkos (orange dot).

The hourly temperature differences between DCC stations, selected a urban station (Pendik) and a rural station (Terkos) which can be seen in Figure 5.5, are calculated as 5K for daytime and 8K for the nighttime, can be seen in Figure 5.7.

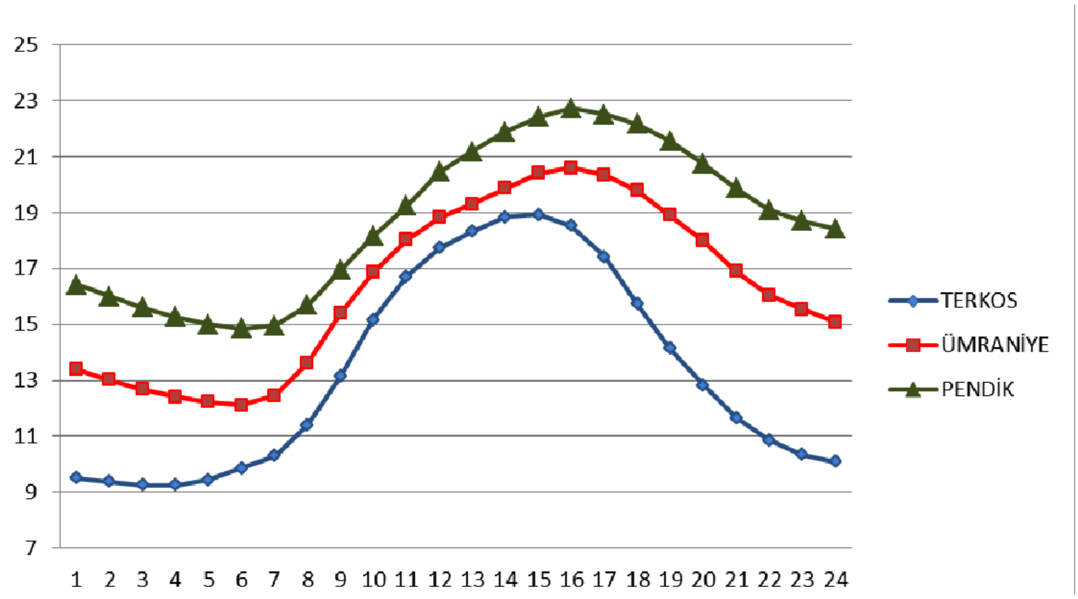

Figure 5.7 : The hourly temperature differences between DCC stations.

5.2 Sensitivity Analysis

In order to determine how to develop the initialization the 1-dimensional simulation of MUKLIMO_3 Thermodynamic Version for Mega City Istanbul, some sensitivity tests according to profile values of wind speed and wind direction have been performed for a typical day. The radiosonde data of 17064 Kartal Station for 02 August 2014 12:00 UTC which is measured bt TSMS. This profile values are essential part for the 1-dimensional simulation which creates the input file for 3-dimensional simulations. Firstly, the outputs for the simulations of 02.08.2014 (default simulation) will be analyzed, secondly, the prepared sensitivity to the wind parameter “wind” and “phiwin” in the name list, will be determined to find the fit for further simulations are done by MUKLIMO_3 for Istanbul. This will be done according to change the wind speed and direction at the 10 m, because the variations of other meteorological variables highly depend on the wind speed, and these are one of the most fundamental parameters for analyzing the urban heat island effect.

In Table 5.2, the parameters of the sensitivity analysis simulations are summarized.

There are one default scenario which is ran by reference profile values, 4 wind direction scenarios (WD) which contain a reference wind speed which is provided by radiosonde data with 4 different wind directions and finally 6 wind speed scenarios (WS) with a reference wind direction at 10 m with 6 different wind speed. The predominant wind directions of Istanbul (northeast and southwest) are considered while selecting the wind directions for these scenarios.

Table 5.2 : The parameters of the sensitivity analysis simulations.

Name	Wind Direction (°)	Wind Speed (m/s)
Reference	10	1.0
WD 1	20	1.0
WD 2	45	1.0
WD 3	200	1.0
WD 4	225	1.0
WS 1	10	2.0
WS 2	10	1.5
WS 3	10	0.5
WS 4	10	2.5
WS 5	10	5.0
WS 6	10	10.0

5.2.1 Sensitivity to wind direction changes

The sensitivity analysis has been done to seek the importance of the wind direction on the urban heat island intensity over Istanbul. Therefore, a reference run has been started first with the default wind direction value *(phiwin=10°)* regarding the Radiosonde Data for the 02 August 2014 12Z. Afterwards, four sensitivity runs with changed values for the wind direction; WD 1 *(phiwin=20°)*, WD 2 *(phiwin45°)*, WD 3 *(phiwin=200°)*, WD 4 *(phiwin=225°)* have all been started using same wind speed *(wind=1 m/s)* from the reference run (Figure 5.8).

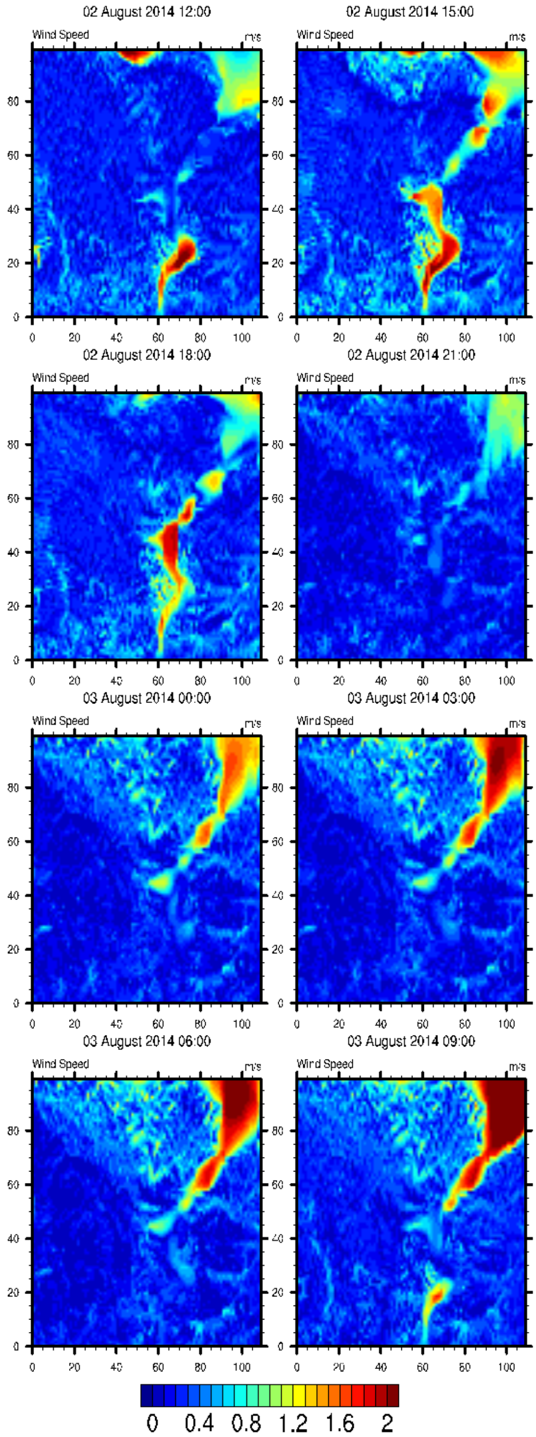

Figure 5.8 : Spatial distribution of wind speed of reference simulation.

(a) WD 1

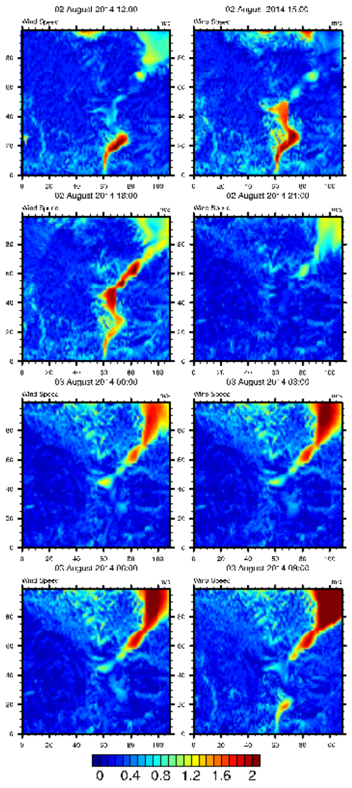

(b) WD 2

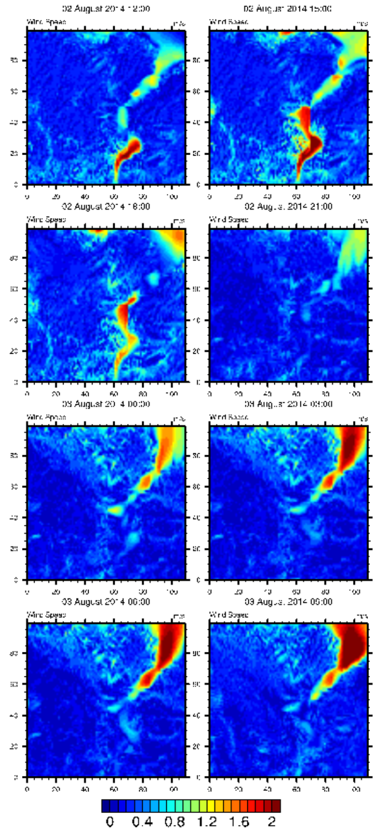

(c) WD 3

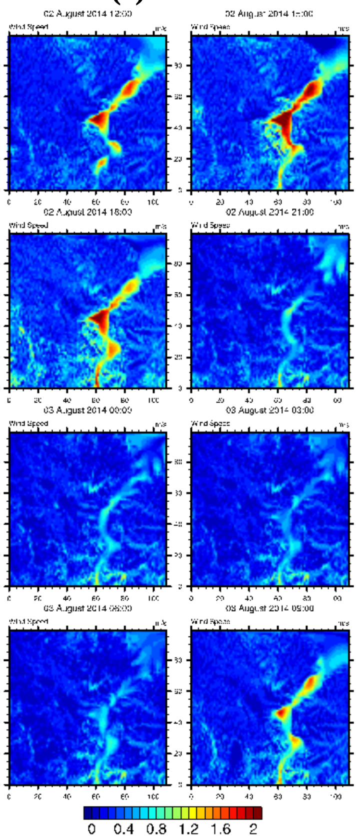

(d) WD 4

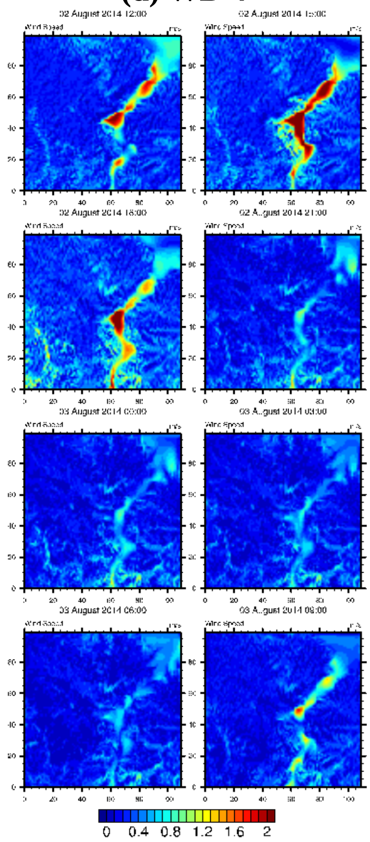

Figure 5.9 : Spatial distribution of changing wind direction of green 2 **(a),** white 3 **(b)**, hybrid 5 **(c)** and hybrid 6 **(d)** scenerios.

The Figure 5.9 shows the simulated wind speed for different prevealing wind directions. Reference run *(phiwin=10°)*, WD 1 *(phiwin=20°)* and WD 2 *(phiwin45°)* represent the northeasterly wind direction scenarios, the other specfications are same as the reference simulation. The channel effect especially nighttime for the north part of the Bosphorus can be seen. Besides, when the model is forced with the southwesterly wind direction (WD 3 *(phiwin=200°)* and WD 4 *(phiwin=225°*)), slightly lighter wind pattern over the Bosphorus is simulated. Both for the northeasterly and southweasterly direction tests, the wind speed is relatively calm over the residential areas since the buildings inhibit the flow and decrease the wind speed.

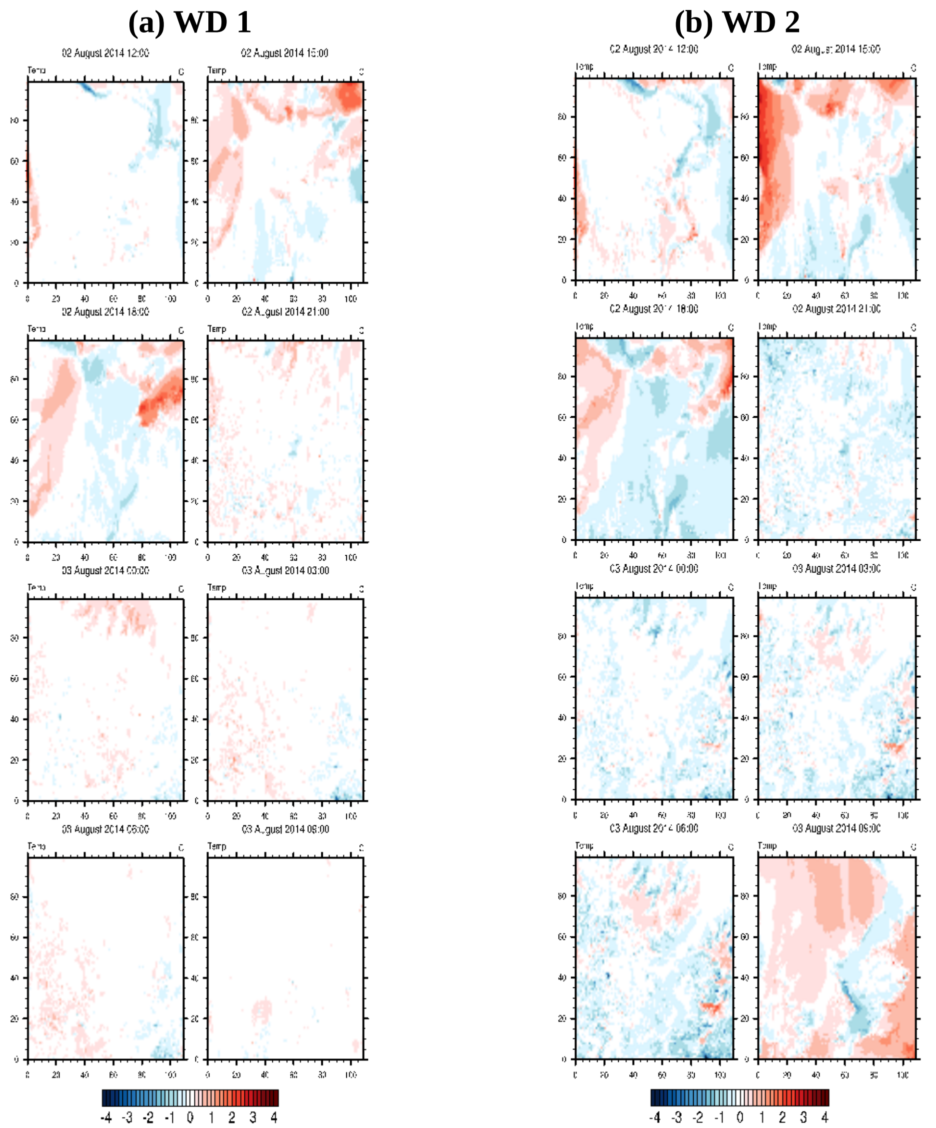

Figure 5.10 : Temperature differences of changing wind direction of WD 1 **(a)** and WD 2 **(b)** scenerios

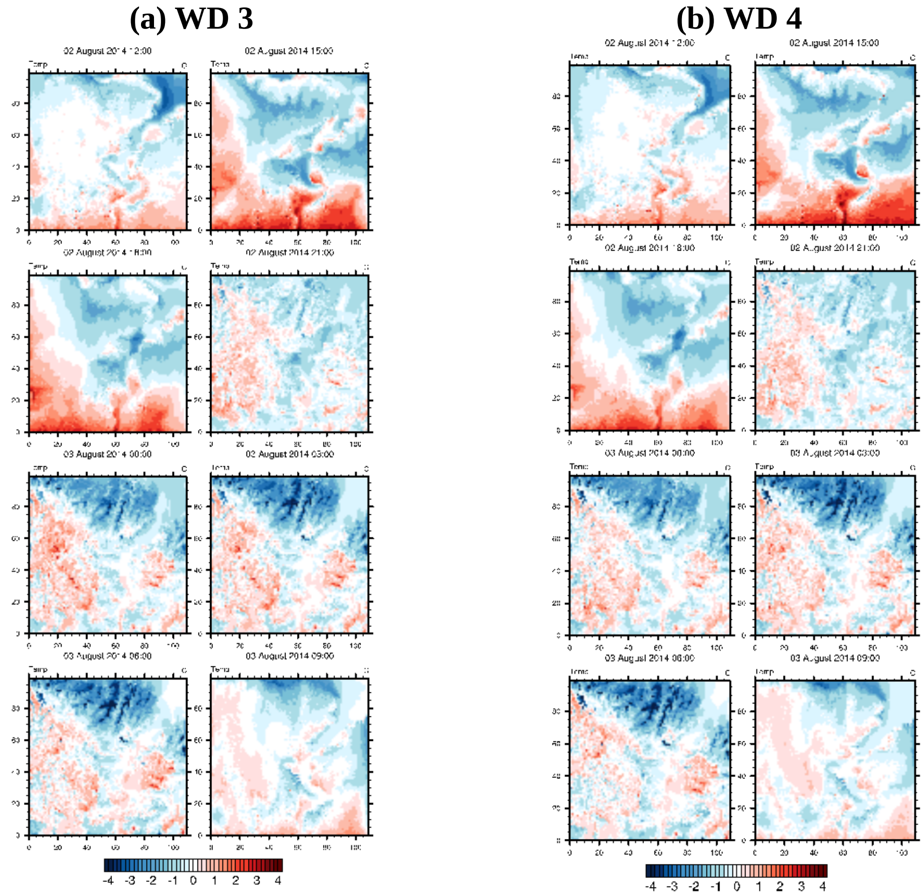

Figure 5.11 : Temperature differences of changing wind direction of WD 3 **(a)** and WD 4 **(b)** scenerios.

Figure 5.11 represent the temperature differences in the sensitivity tests compared to the reference simulation. It emphasizes that the simulation results show that WD 3 *(phiwin=200°)* and WD 4 *(phiwin=225°*), which are the southwesterly wind scenarios have negative biases (cooling effect) for the northern part of the domain and positive biases (warming effect) for the southern part. WD 1 *(phiwin=20°)* and WD 2 *(phiwin45°)* analyses (Figure 5.10) represent the northeasterly wind direction same as the reference simulation. Therefore, the scenerios of WD 1 and WD 2 are less effective than WD 3 and WD 4 and the sensitivity of the urban are not as striking as the third and fourth tests.

5.2.2 Sensitivity to wind speed changes

The sensitivity of the urban heat island intensity to wind speeds is accomplished by changing the wind speed parameter “wind”. Therefore, a reference run (Figure 5.12) has been started first with the reference wind speed value *(wind=1.0 m/s)* regarding the Radiosonde Data for the 02 August 2014 12:00 UTC. Afterwards, six sensitivity runs with changed values for the wind speed; WS 1 *(wind=2.0 m/s)*, WS 2 *(wind=1.5 m/s)*, WS 3 *(wind=0.5 m/s)*, WS 4 *(wind=2.5 m/s)*, WS 5 *(wind=5.0 m/s)*, WS 6 *(wind=10.0 m/s)*, have all been started using the same wind direction *(phiwin=10°)* from the reference run with a profile values.

The Figure 5.13 shows the sensitivity test of increasing (WS 1 *(wind=2.0 m/s)*, WS 2 *(wind=1.5 m/s)*, WS 4 *(wind=2.5 m/s)*, WS 5 *(wind=5.0 m/s)*, WS 6 *(wind=10.0 m/s)* and decreasing (WS 3 *(wind=0.5 m/s))* the wind speed. On the other hand, an increase in the wind speed leads to stronger channel effect especially during the night.

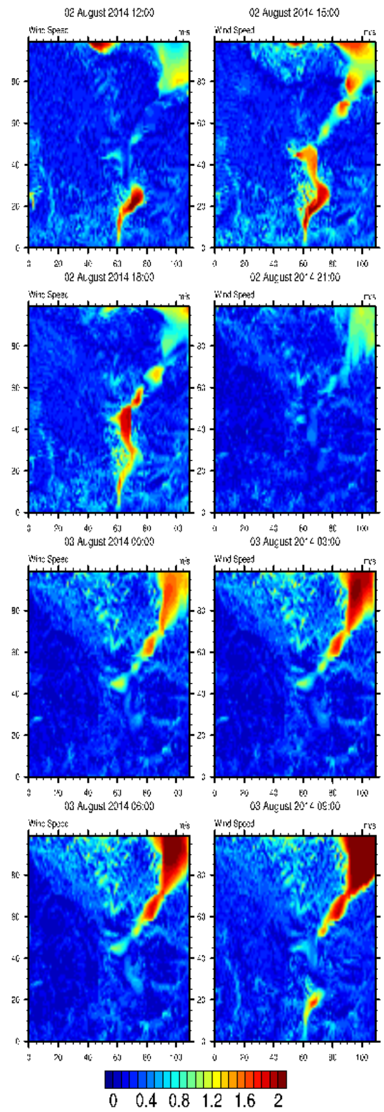

Figure 5.12 : Spatial distribution of wind speed of reference simulation.

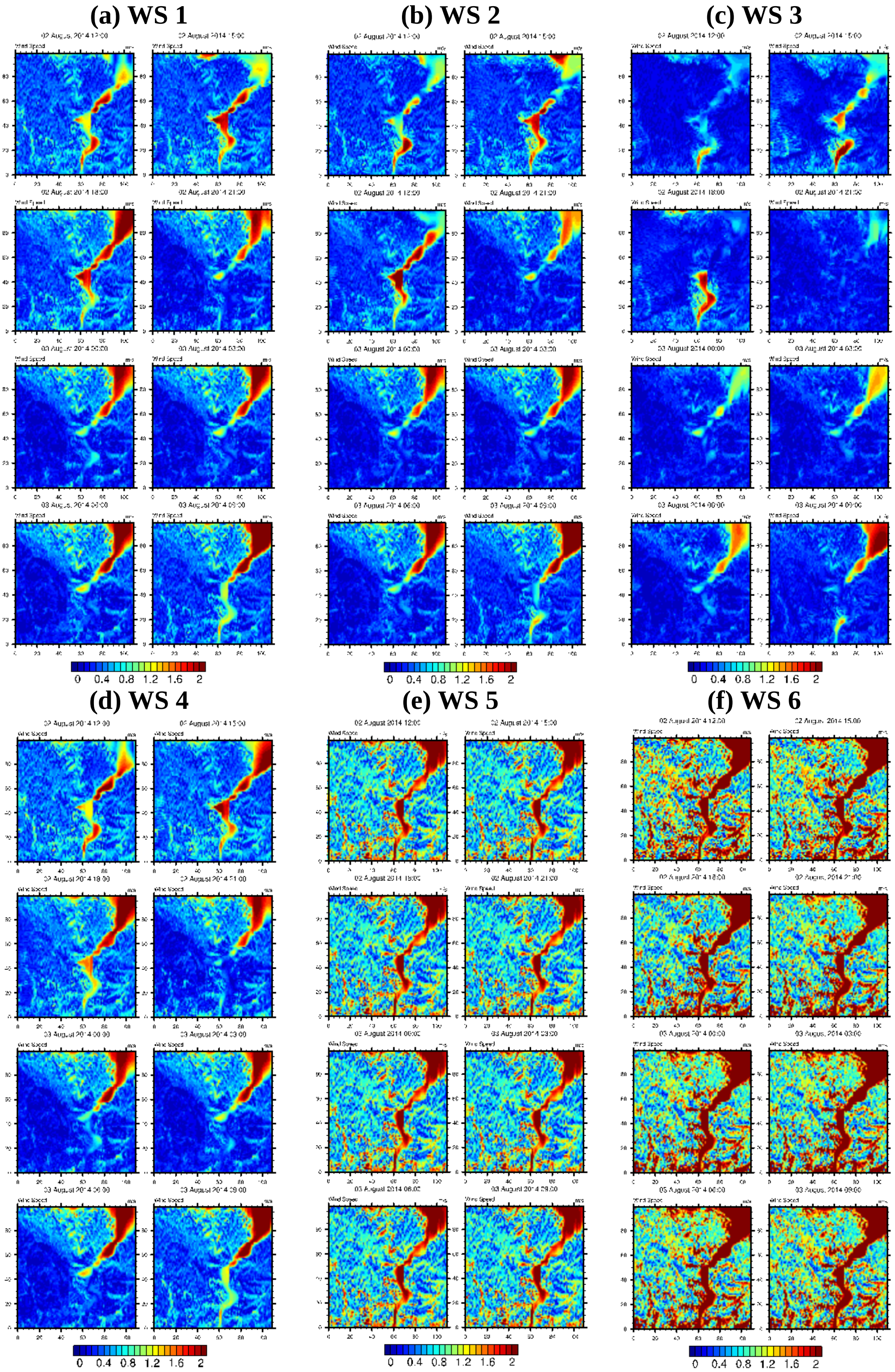

Figure 5.13 : Spatial distribution of changing wind speed of WS 1 **(a),** WS 2 **(b),** WS 3 **(c),** WS 4 **(d),** WS 5 **(e)** and WS 6 **(f)** scenerios.

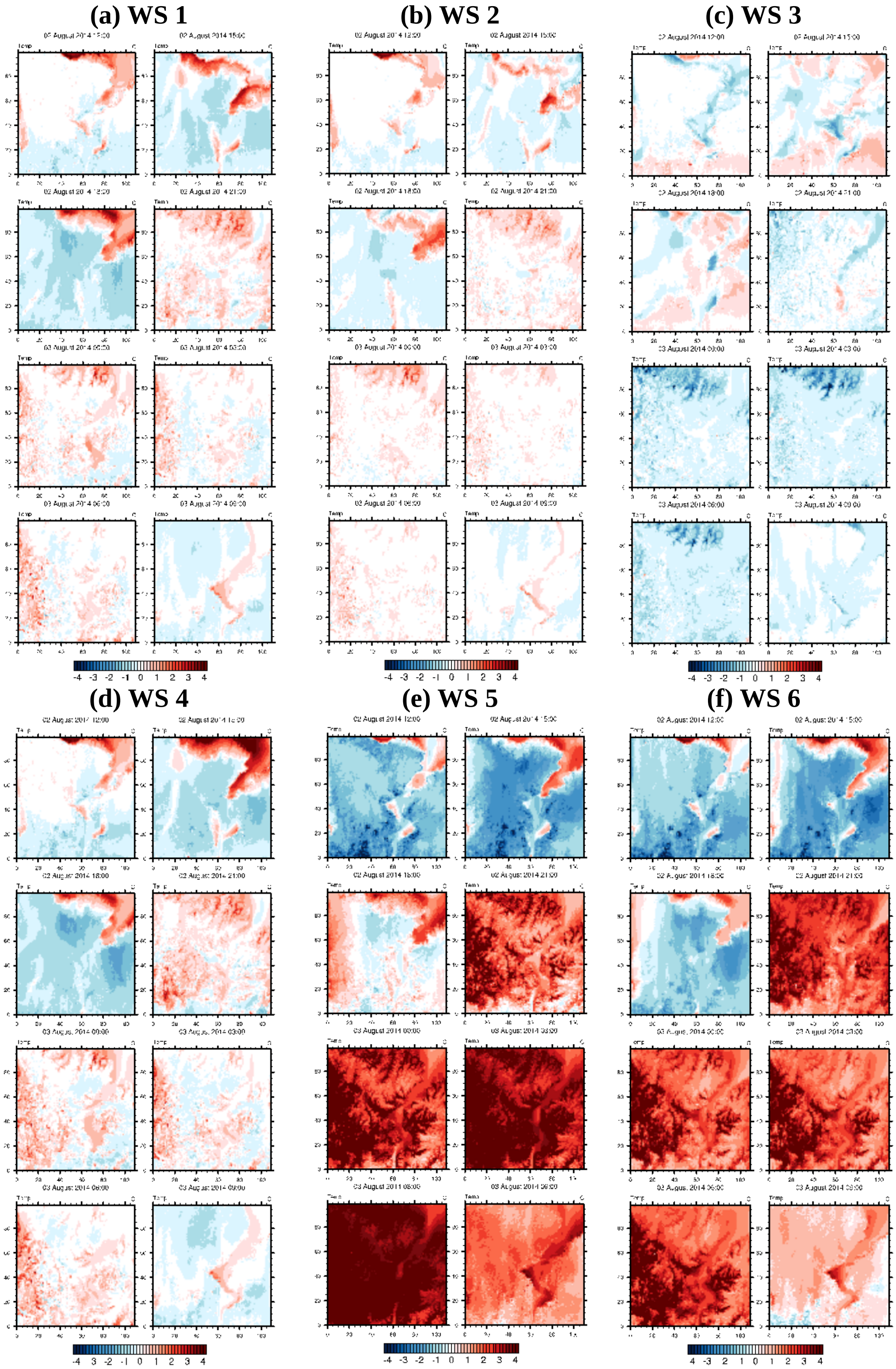

Figure 5.14 : Temperature differences of changing wind speed for WS 1 **(a),** WS 2 **(b),** WS 3 **(c),** WS 4 **(d),** WS 5 **(e)** and WS 6 **(f)** scenerios.

Figure 5.14 shows that all the sensitivity tests to wind speed changes (WS 1 *(wind=2.0 m/s)*, WS 2 *(wind=1.5 m/s)*, WS 4 *(wind=2.5 m/s)*, WS 5 *(wind=5.0 m/s)*, WS 6 *(wind=10.0 m/s)*) which have stronger wind speed than the reference simulation except WS 3 *(wind=0.5 m/s)*, have negative differences (cooling effect) for the southern part of the domain besides have positive differences (warming effect) for the northern part for the daytime simulations. The warming effect both for the rural and urban areas is high especially for the 21:00, 00:00, 03:00 and 06:00 simulations. An increase in the speed leads to higher temperatures ar 2 m during the night due to increased mixing height. Even though the surface cools down due to the emitted infrared radiation, the cooled air neaby the surface is mixing up with the air aloft resulting less temperature drops at 2 m height compared to the calm conditions. Besides rapid release of heat from the buildings in the moderate wind conditions enhances the urban heat island effect. The distribution of the nighttime temperature changes in the WS 5 runs is similar to WS 6 and these tests have the higher positive differences and estimate warmer nocturnal temperature over the residential areas. On the other hand, the only WS 3 *(wind=0.5 m/s)* scenario which have slightly lighter wind speed than the reference profile value *(wind=1.0 m/s)* have visibly strong cooling effect in comparison with the other tests *(WS 1, WS 2, WS 4, WS 5, WS 6.*

5.3 Scenarios

In this work, the implementation of several mitigation strategies (green roofs, high-albedo materials and the combination of them as hybrid) are considered in order to lower the temperatures in the urban areas and Istanbul City Development Scenarios are developed in order to evaluate the effects of the land use modifications over the city. Due to the fact that MULIMO_3 Thermodynamic Version provides the opportunity to implement green roofs as well as high-albedo materials in built-up areas easily by the help of adjusting the related parameters in the land use table, only these two mitigation strategies and the combination of these for a specified land use classes will be simulated in this thesis.

5.3.1 Mitigation strategies

As it has been mentioned in the previous chapters, the urban heat island has a direct effect on human health and welfare due to higher temperature, which is responsible for the heat stroke and mortality risks. Governments, urban planners and residents have to seek practical approaches to improve urban heat mitigation at least cost as adaptation to global warming, extreme heat events and urban heat effects as soon as possible. The planning and policies for urban environmental sustainability in the metropolitan area of Istanbul are impossible without a temperature mitigation policy and sufficient conscious.

In order to mitigate the urban heat load over cities, in general two different approaches are used. Firstly, one could increase the albedo rate of urban structures such as streets, walls and roofs, to reflect the incoming solar radiation in order to prevent heat storage in urban areas (Rosenfeld et al., 1998; Synnefa et al., 2008). Using high reflective coating or whiter materials for the rooftops and the wall areas should be considered to reduce the atmospheric heating and building energy savings through an increase in albedo. The other approach is greenery, which is a useful mitigation strategy to reduce the UHI by cooling the ambient air and providing milder outdoor boundary conditions (Sodoudi et al., 2014). This can be achieved by increasing the individual green areas like building new parks, a big park or many small parks distributed throughout the city. However the structure of Istanbul is not suitable for increasing park and forested area, since the urban sprawl and lack of free space to convert into green areas. Therefore considering green roofs and walls may provide efficient mitigation of excessive heat load in Istanbul.

Many researches have been focused on comparing the advantages of green and cool roofs in terms of building energy efficiency and rooftop microclimates. Takebayashi and Moriyama (2007), compared and investigated the effectiveness of green and white roofs in Kobe, Japan. They confirmed that, peak sensible heat fluxes (Q_H) were 153 W/m^2, which is relatively small for the white roofs due to the low net radiation (Q*) achieved by high solar reflectance during the daytime. Q_H was 361 W/m^2, which was also relatively small on the green roofs because of the large evapotranspiration (Q_E), which peaked between 400 and 600 W/m^2. However, despite the energy spent for evapotranspiration, Q_H of the green roof was still more than twice as high as the white roof. In a review of green and white roof effectiveness, Santamouris (2014), assumed that, when the albedo of reflective roofs is 0.7 or higher, cool roofs present a higher mitigation potential compared to green roofs with vegatation. Addition to Takebayashi and Moriyama's study, Scherba et al.

(2011) determined the efficiencies of these two mitigation ways. They evaluated the performance of green and white roofs, finding that daytime Q_H was similar, whereas the total daily Q_H was considerably higher for green roofs since the thermal mass of the green roof maintained Q_H positive at night.

In order to investigate what type of changes in the urban landscape elevate the intensity of UHI in Istanbul, by using these dry days, the effects of change in land use on daytime and nighttime urban heat island (UHI) of Istanbul is examined using the micro-scale climate model MUKLIMO 3. A Case domain for Maslak (shown in Figure 5.15) and date (07/08/2012) are selected and the implementation of green roofs and high-albedo materials are considered in order to lower the temperature. Due to the fact that MULIMO_3 provides the opportunity to implement green roofs as well as high-albedo materials in built-up areas and their combination, 11 mitigation strategies with 3 scenarios per strategy are applied.

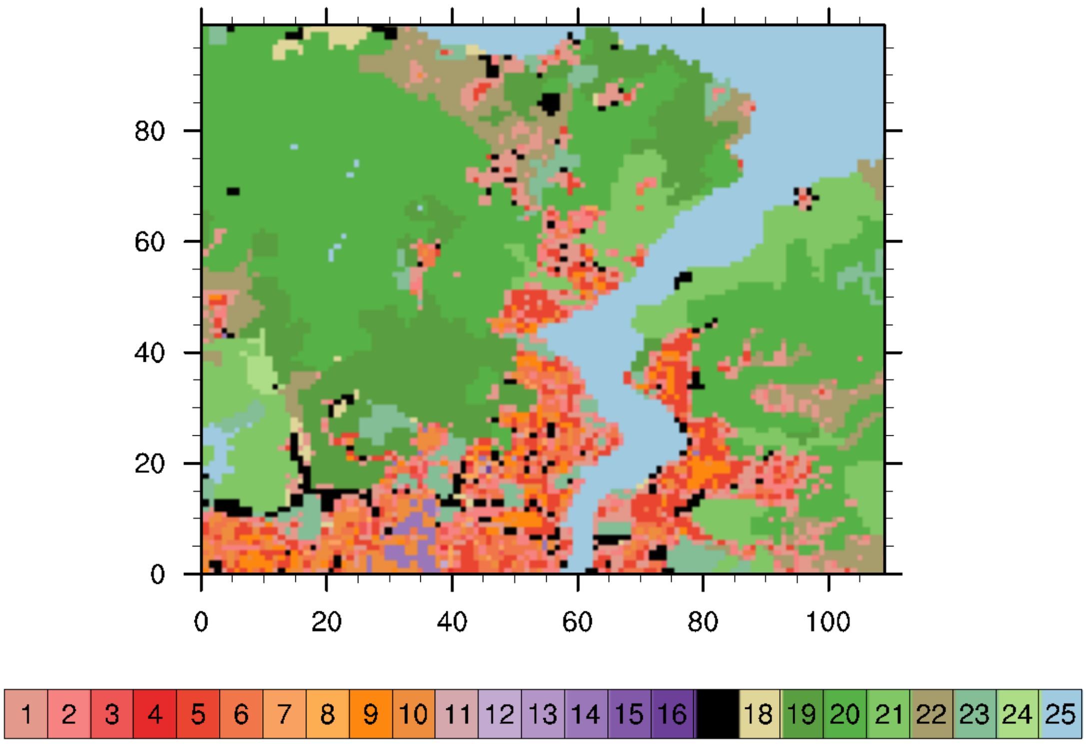

Figure 5.15 : Land use classes and domain for Maslak, Istanbul.

In **Table 5.3**, the parameters of the mitigation simulations are summarized. There are 2 green, 3 white and 6 hybrid scenarios, which represent the possible combinations of the green and cool surfaces. These 11 scenarios are applied for whole residential area, whereas more detailed simulations are needed to observe the changes of microclimate. Therefore, more specific cases are implemented; the scenarios are indicated with the "a" represent that the parameter changes are only applied for areas with high-rise buildings which are shown with the number 4, 8, 12 and 16 in the land use table and the scenarios with "b" show the simulations only include the high dense residential area which are represedented by number 13, 14, 15 and 16 in the land use table.

Table 5.3 : The parameters of the mitigation simulations.

Name	Green Roof Fraction (Grant)	Albedo of Walls (Albw)	Albedo of Roofs (Albd)
Reference	0	0.3	0.2
White 1	0	0.5	0.5
White 1a	0	0.5	0.5
White 1b	0	0.5	0.5
White 2	0	0.7	0.7
White 2a	0	0.7	0.7
White 2b	0	0.7	0.7
White 3	0	0.9	0.9
White 3a	0	0.9	0.9
White 3b	0	0.9	0.9
Green 1	0.3	0.3	0.2
Green 1a	0.3	0.3	0.2
Green 1b	0.3	0.3	0.2
Green2	0.7	0.3	0.2
Green2a	0.7	0.3	0.2
Green2b	0.7	0.3	0.2
Hybrid 1	0.3	0.5	0.5
Hybrid 1a	0.3	0.5	0.5
Hybrid 1b	0.3	0.5	0.5
Hybrid 2	0.3	0.7	0.7
Hybrid 2a	0.3	0.7	0.7
Hybrid 2b	0.3	0.7	0.7
Hybrid 3	0.7	0.5	0.5
Hybrid 3a	0.7	0.5	0.5
Hybrid 3b	0.7	0.5	0.5
Hybrid 4	0.7	0.7	0.7
Hybrid 4a	0.7	0.7	0.7
Hybrid 4b	0.7	0.7	0.7
Hybrid 5	0.3	0.9	0.9
Hybrid 5a	0.3	0.9	0.9
Hybrid 5b	0.3	0.9	0.9
Hybrid 6	0.7	0.9	0.9
Hybrid 6a	0.7	0.9	0.9
Hybrid 6b	0.7	0.9	0.9

Grant defines the fraction of green roofs in each land use class with buildings, while the reference value is 0. *Albw* and *albd* determine the albedo of the walls and roofs with reference values 0.3 and 0.2, respectively. Žuvela-Aloise et al. (2015) simulated with albedo values 0.5, 0.7 and 0.9 and Kniebusch (2015) run the model with green roof fraction values 0.3 and 0.7. The values of scenarios for this study are chosen with regard to these researches.

5.3.1.1 Mean temperature reduction

As it has been mentioned before, using high albedo materials such as white coating and bright asphalt for the built-up areas reduce the amount of incoming solar radiation absorbed through urban structures and thus keep their surfaces cooler (Sodoudi, 2014). Besides, greenery reduced solar radiation too and lowered near-surface air temperature due to evapotranspiration.

The mean temperature differences for each mitigation strategy as a diurnal variation is shown in Figure 5.16. Green, white and hybrid scenarios were applied to urban areas which are represented by buildings (land use class no. 1-16) and substracted from the reference simulation. By comparison with the current simulation, all the scenarios have cooler effects and peak during the daytime. It is obvious that these scenarios mitigate the 2 m temperature since the high reflectivity of the white urban structure and the high evapotranspiration of the green roofs during the day when the temperature reaches its maximum, whereas the reduction in 2 m temperature during the night is quite small.

Modifying the rooftop surface through implementation of green or cool roofs both alters surface atmosphere interactions and the resulting roof microclimate. Additionally, using green roofs do not have significant cooling effect compared to white roofs and this result was demonstrated by Santamouris (2014), assumed that when the albedo of cool roofs is 0.7 or more, high reflected roofs present a higher mitigation potential compared to green roofs.

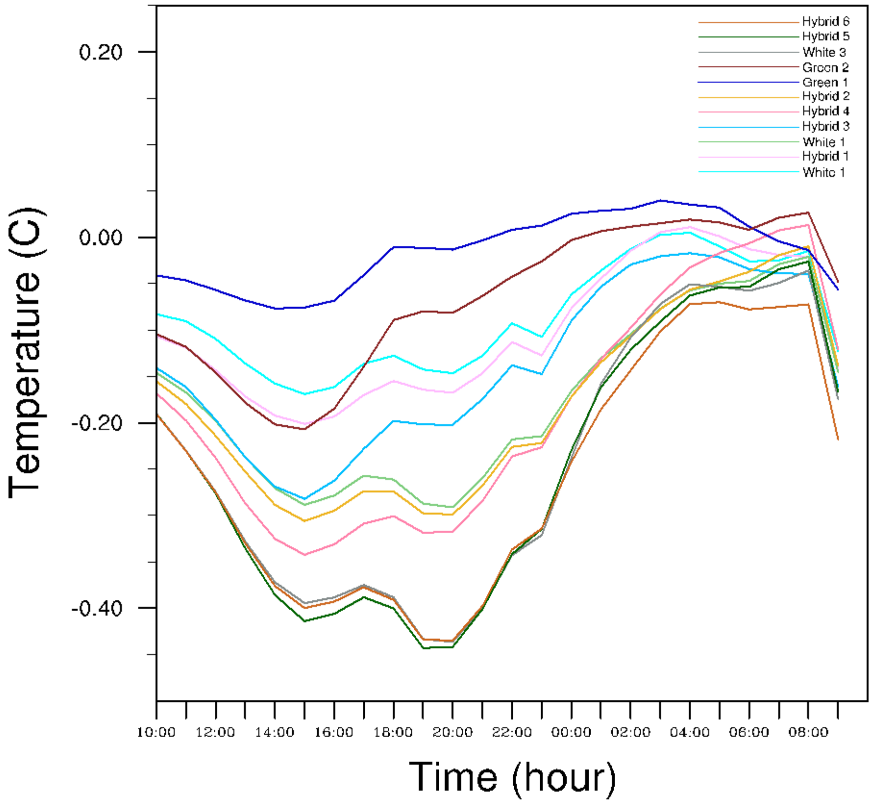

Figure 5.16 : Diurnal variation of mitigation strategies.

Figure 5.16, indicates that the effectiveness of the green roof scenarios are less than the white and hybrid scenarios. The mitigation potential of “Green 1” scenario is almost 0K, however the “White 3”, “Hybrid 5” and “Hybrid 6” scenarios reach approximately -0.5K cooling effect around 19:00. On the other hand the “Hybrid 5” *(grant=0.3 albw=0.9)* have the most considerable cooling effect during the daytime, whereas have less cooling effect than the “Hybrid 6” *(grant=0.7 albw=9)* scenario during the nighttime. Likewise, during the night, when urban heat island is commonly at its maximum, green roofs seem to cause positive temperature anomalies compared to the other scenarios.

Table 5.4 : The hourly mean temperature changes for each mitigation scenarios.

Time	W1-R.	W2-R.	W3-R.	G1-R.	G2-R.	H1-R.	H2-R.	H3-R.	H4-R.	H5-R.	H6-R.
10:00	-0.08	-0.15	-0.19	-0.04	-0.1	-0.11	-0.16	-0.14	-0.17	-0.19	-0.19
11:00	-0.09	-0.17	-0.23	-0.05	-0.12	-0.12	-0.18	-0.16	-0.2	-0.23	-0.23
12:00	-0.11	-0.2	-0.27	-0.06	-0.15	-0.14	-0.21	-0.2	-0.24	-0.28	-0.28
13:00	-0.14	-0.24	-0.33	-0.07	-0.18	-0.17	-0.25	-0.24	-0.29	-0.34	-0.33
14:00	-0.16	-0.27	-0.37	-0.08	-0.2	-0.19	-0.29	-0.27	-0.33	-0.39	-0.38
15:00	-0.17	-0.29	-0.39	-0.08	-0.21	-0.2	-0.31	-0.28	-0.34	-0.41	-0.4
16:00	-0.16	-0.28	-0.39	-0.07	-0.18	-0.19	-0.29	-0.26	-0.33	-0.41	-0.39
17:00	-0.14	-0.26	-0.38	-0.04	-0.14	-0.17	-0.27	-0.23	-0.31	-0.39	-0.38
18:00	-0.13	-0.26	-0.39	-0.01	-0.09	-0.16	-0.27	-0.2	-0.3	-0.4	-0.39
19:00	-0.14	-0.29	-0.43	-0.01	-0.08	-0.16	-0.3	-0.2	-0.32	-0.44	-0.43
20:00	-0.15	-0.29	-0.44	-0.01	-0.08	-0.17	-0.3	-0.2	-0.32	-0.44	-0.43
21:00	-0.13	-0.26	-0.4	0	-0.06	-0.15	-0.27	-0.17	-0.28	-0.4	-0.4
22:00	-0.09	-0.22	-0.34	0.01	-0.04	-0.11	-0.23	-0.14	-0.24	-0.34	-0.34
23:00	-0.11	-0.21	-0.32	0.01	-0.03	-0.13	-0.22	-0.15	-0.23	-0.31	-0.31
0:00	-0.06	-0.17	-0.24	0.03	0	-0.08	-0.17	-0.09	-0.17	-0.23	-0.24
1:00	-0.04	-0.13	-0.16	0.03	0.01	-0.04	-0.13	-0.05	-0.13	-0.16	-0.19
2:00	-0.01	-0.1	-0.11	0.03	0.01	-0.01	-0.11	-0.03	-0.1	-0.12	-0.14
3:00	0	-0.08	-0.07	0.04	0.02	0.01	-0.08	-0.02	-0.06	-0.09	-0.1
4:00	0.01	-0.06	-0.05	0.04	0.02	0.01	-0.06	-0.02	-0.03	-0.06	-0.07
5:00	-0.01	-0.05	-0.05	0.03	0.02	0	-0.05	-0.02	-0.02	-0.05	-0.07
6:00	-0.03	-0.05	-0.06	0.01	0.01	-0.01	-0.04	-0.03	-0.01	-0.05	-0.08
7:00	-0.02	-0.03	-0.05	0	0.02	-0.02	-0.02	-0.04	0.01	-0.03	-0.08
8:00	-0.01	-0.02	-0.04	-0.01	0.03	-0.02	-0.01	-0.04	0.01	-0.03	-0.07
9:00	-0.12	-0.14	-0.17	-0.06	-0.05	-0.14	-0.14	-0.16	-0.12	-0.17	-0.22
Daily	**-0.087**	**-0.176**	**-0.245**	**-0.015**	**-0.065**	**-0.103**	**-0.182**	**-0.139**	**-0.188**	**-0.248**	**-0.256**

In Table 5.4, the hourly mean temperature changes for each mitigation scenarios are summarized. The last row of this table represents the daily differences of these scenarios and the red boxes indicate the most significant values. The mean cooling effect of the green roofs amounts to 0.015K and 0.065K for 30% and 70%, respectively. The increase in the albedo of the walls and the buildings leads to temperature changes of -0.087K, -0.176K and -0.245K, which is about 3 to 4 times the effect of the green roofs. However the combination of these scenarios which is represented by “Hybrid 6” has less cooling effect then the total amount of the “White 3” and “Green 2”, since the effectiveness of the cool roofs are higher separately so combining this scenario with the greenery reduced the mitigation potential of them. On the other hand, the daily value of “Hybrid 5” is so close to “Hybrid 6” although the “grant” parameter of “Hybrid 5” is 0.4 less then the “Hybrid 6”s.

In Table 5.4, one can see that “Hybrid 5” and “Hybrid 6” are the most effective hybrid scenarios with cooling effects of 0.248K and 0.256K, although the former research of Kniebusch (2015), demonstrates that the higher white scenario is slightly better than hybrids, the results of this study are not in line with the previous studies. Due to the fact that these hybrids have the highest albedo values and that “Hybrid 5”, which has the smaller green scenario, simulates the lower cooling effect rather than the “Hybrid 6”. However, the combination of these scenarios which is represented by “Hybrid 6” has less cooling effect then the total amount of the “White 3” and “Green 2”, since the effectiveness of the cool roofs are higher separately so combining this scenario with the greenery reduced the mitigation potential of them. On the other hand, the daily value of “Hybrid 5” is so close to “Hybrid 6” although the “grant” parameter of “Hybrid 5” is 0.4 less then the “Hybrid 6”s. These facts, emphasize how effective the high-albedo materials are compared to green roofs.

The mean temperature differences for each mitigation strategy as a diurnal variation for built-up area is shown in Figure 5.17. Green, white and hybrid scenarios were applied to urban areas which are represented by buildings (land use class no. 1-16), dimensionally avaraged for only built-up areas and substracted from the reference simulation. By comparison with the current simulation, all the scenarios have cooler effects and peak during the daytime same as the previous plot Figure 5.16.

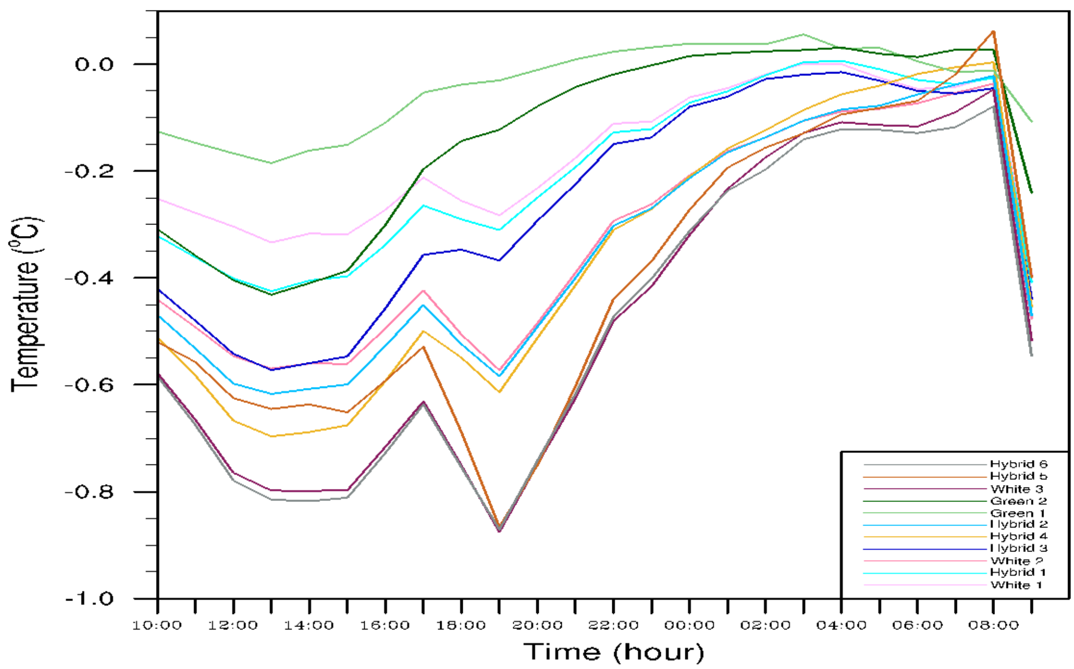

Figure 5.17 : Diurnal variation of mitigation strategies for built-up areas.

Figure 5.17 indicates that the white and hybrid scenarios are more effective than the green roof scenarios. The mitigation potential of “Green 1” scenario is almost 0K, however the cooling effect of “White 3”, “Hybrid 5” and “Hybrid 6” scenarios have a striking peaks around 19:00 and reach approximately -0.9K. On the other hand the “Hybrid 6” *(grant=0.7 albw=0.9)* have the most considerable cooling effect during both the daytime and nighttime. Likewise, during the night, when urban heat island is commonly at its maximum, “Green 1” and “Green 2” seem to cause positive temperature anomalies compared to the other scenarios. More suprisingly, “Hybrid 5” scenario has a striking peak around 08:00 and reaches approximately 0.1K.

In Table 5.5, the hourly mean temperature changes for each mitigation scenarios for built-up area are summarized.

Table 5.5 : The hourly mean temperature changes for each mitigation scenarios of built-up areas.

Time	W1-R.	W2-R.	W3-R.	G1 - R.	G2 - R.	H1 - R.	H2 - R.	H3 - R.	H4 - R.	H5 - R.	H6 - R.
10:00	-0.25	-0.44	-0.58	-0.13	-0.31	-0.32	-0.47	-0.42	-0.51	-0.52	-0.58
11:00	-0.28	-0.49	-0.67	-0.15	-0.36	-0.36	-0.53	-0.48	-0.58	-0.56	-0.67
12:00	-0.3	-0.55	-0.76	-0.17	-0.4	-0.4	-0.6	-0.54	-0.67	-0.63	-0.78
13:00	-0.33	-0.57	-0.8	-0.18	-0.43	-0.42	-0.62	-0.57	-0.7	-0.65	-0.81
14:00	-0.32	-0.56	-0.8	-0.16	-0.41	-0.4	-0.61	-0.56	-0.69	-0.64	-0.82
15:00	-0.32	-0.56	-0.8	-0.15	-0.39	-0.4	-0.6	-0.55	-0.68	-0.65	-0.81
16:00	-0.27	-0.49	-0.72	-0.11	-0.3	-0.34	-0.53	-0.46	-0.59	-0.59	-0.73
17:00	-0.21	-0.42	-0.63	-0.05	-0.2	-0.26	-0.45	-0.36	-0.5	-0.53	-0.64
18:00	-0.26	-0.51	-0.75	-0.04	-0.14	-0.29	-0.52	-0.35	-0.55	-0.69	-0.75
19:00	-0.28	-0.57	-0.88	-0.03	-0.12	-0.31	-0.58	-0.37	-0.61	-0.87	-0.87
20:00	-0.23	-0.48	-0.75	-0.01	-0.08	-0.25	-0.49	-0.29	-0.51	-0.75	-0.74
21:00	-0.18	-0.39	-0.63	0.01	-0.04	-0.19	-0.4	-0.22	-0.41	-0.6	-0.62
22:00	-0.11	-0.29	-0.48	0.02	-0.02	-0.13	-0.3	-0.15	-0.31	-0.44	-0.47
23:00	-0.11	-0.26	-0.42	0.03	0	-0.12	-0.27	-0.14	-0.27	-0.37	-0.4
0:00	-0.06	-0.21	-0.32	0.04	0.02	-0.07	-0.21	-0.08	-0.21	-0.27	-0.31
1:00	-0.04	-0.16	-0.23	0.04	0.02	-0.05	-0.17	-0.06	-0.16	-0.19	-0.24
2:00	-0.02	-0.14	-0.17	0.04	0.02	-0.02	-0.14	-0.03	-0.12	-0.16	-0.2
3:00	0	-0.11	-0.13	0.06	0.03	0	-0.11	-0.02	-0.09	-0.13	-0.14
4:00	0	-0.09	-0.11	0.03	0.03	0.01	-0.08	-0.01	-0.06	-0.09	-0.12
5:00	-0.03	-0.08	-0.11	0.03	0.02	-0.01	-0.08	-0.03	-0.04	-0.08	-0.12
6:00	-0.05	-0.07	-0.12	0.01	0.01	-0.03	-0.06	-0.05	-0.02	-0.07	-0.13
7:00	-0.04	-0.05	-0.09	-0.01	0.03	-0.04	-0.04	-0.05	-0.01	-0.02	-0.12
8:00	-0.02	-0.04	-0.05	-0.01	0.03	-0.03	-0.02	-0.04	0	0.06	-0.08
9:00	-0.39	-0.48	-0.52	-0.11	-0.24	-0.41	-0.47	-0.44	-0.45	-0.4	-0.55
Daily	**-0.171**	**-0.334**	**-0.480**	**-0.042**	**-0.135**	**-0.202**	**-0.348**	**-0.261**	**-0.364**	**-0.410**	**-0.488**

The last row of this table represents the daily differences of these scenarios and the red boxes indicate the most significant values. The mean cooling effect of the green roofs are between 0.042K and 0.135K for 30% and 70%, respectively. The increase in the albedo of the walls and the buildings leads to temperature changes of -0.171K, -0.334K and -0.480K, which is about 3 to 4 times the effect of the green roofs. As is the case with the previous Table 5.4, the combination of these scenarios which is represented by “Hybrid 6” has less cooling effect then the total amount of the “White 3” and “Green 2”, since the effectiveness of the cool roofs are higher separately so combining this scenario with the greenery reduced the mitigation potential of them. On the other hand, the daily value of “Hybrid 5” is so close to “Hybrid 6” although the “grant” (green roof fraction) parameter of “Hybrid 5” is 0.4 less then the “Hybrid 6”s. Therefore, the contribution of green roofs can be classified as negliable for the hybrid scenarios since the slight variation between them.

The mean temperature differences for each mitigation strategy as a diurnal variation for non built-up area is shown in Figure 5.18. Green, white and hybrid scenarios were applied to study area, dimensionally avaraged for only non built-up areas and substracted from the reference simulation. By comparison with the current simulation, all the scenarios have cooling effects and peaks during the daytime and the 2 m temperature differences between the strategies and the reference simulation decrease during the nighttime same as the previous plots Figure 5.16 and Figure 5.17.

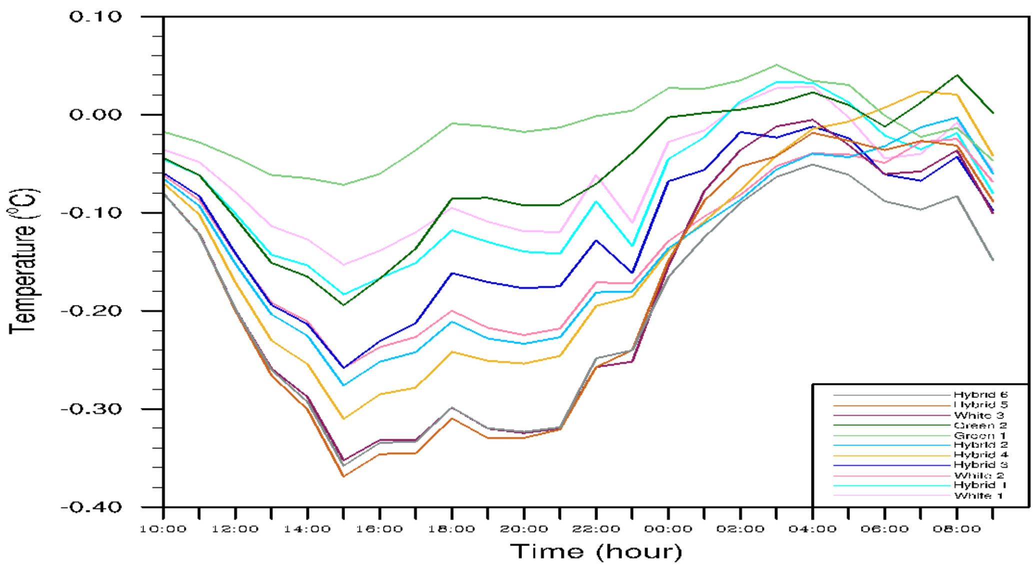

Figure 5.18 : Diurnal variation of mitigation strategies for non built-up areas.

Figure 5.18, indicates that the effectiveness of white and hybrid scenarios are more than the green roof scenarios again. The mitigation potential of “Green 1” scenario is almost 0K, however the cooling effect of “White 3”, “Hybrid 5” and “Hybrid 6” scenarios have peak around 15:00 and reach approximately -0.36K around 19:00. On the other hand the “Hybrid 6” *(grant=0.7 albw=0.9)* have the most considerable cooling effect during daytime. Likewise, during the night, when urban heat island is commonly at its maximum, “Green 1” scenario seems to cause positive temperature anomalies compared to the other scenarios.

Table 5.6 : The hourly mean temperature changes for each mitigation scenarios of non built-up areas.

Time	W1-R.	W2-R.	W3-R.	G1-R.	G2-R.	H1-R.	H2-R.	H3-R.	H4-R.	H5-R.	H6-R.
10:00	-0.04	-0.06	-0.08	-0.02	-0.04	-0.05	-0.07	-0.06	-0.07	-0.08	-0.08
11:00	-0.05	-0.09	-0.12	-0.03	-0.06	-0.06	-0.09	-0.08	-0.1	-0.12	-0.12
12:00	-0.08	-0.14	-0.2	-0.04	-0.11	-0.1	-0.15	-0.14	-0.17	-0.2	-0.2
13:00	-0.11	-0.19	-0.26	-0.06	-0.15	-0.14	-0.2	-0.19	-0.23	-0.27	-0.26
14:00	-0.13	-0.21	-0.29	-0.06	-0.17	-0.15	-0.23	-0.21	-0.25	-0.3	-0.29
15:00	-0.15	-0.26	-0.35	-0.07	-0.19	-0.18	-0.28	-0.26	-0.31	-0.37	-0.36
16:00	-0.14	-0.24	-0.33	-0.06	-0.17	-0.17	-0.25	-0.23	-0.29	-0.35	-0.33
17:00	-0.12	-0.23	-0.33	-0.04	-0.14	-0.15	-0.24	-0.21	-0.28	-0.35	-0.33
18:00	-0.1	-0.2	-0.3	-0.01	-0.09	-0.12	-0.21	-0.16	-0.24	-0.31	-0.3
19:00	-0.11	-0.22	-0.32	-0.01	-0.08	-0.13	-0.23	-0.17	-0.25	-0.33	-0.32
20:00	-0.12	-0.22	-0.32	-0.02	-0.09	-0.14	-0.23	-0.18	-0.25	-0.33	-0.32
21:00	-0.12	-0.22	-0.32	-0.01	-0.09	-0.14	-0.23	-0.18	-0.25	-0.32	-0.32
22:00	-0.06	-0.17	-0.26	0	-0.07	-0.09	-0.18	-0.13	-0.2	-0.26	-0.25
23:00	-0.11	-0.17	-0.25	0	-0.04	-0.13	-0.18	-0.16	-0.19	-0.24	-0.24
0:00	-0.03	-0.13	-0.15	0.03	0	-0.05	-0.14	-0.07	-0.14	-0.15	-0.17
1:00	-0.02	-0.1	-0.08	0.03	0	-0.02	-0.11	-0.06	-0.11	-0.09	-0.13
2:00	0.01	-0.08	-0.04	0.03	0	0.01	-0.09	-0.02	-0.08	-0.05	-0.09
3:00	0.03	-0.05	-0.01	0.05	0.01	0.03	-0.06	-0.02	-0.04	-0.04	-0.06
4:00	0.03	-0.04	-0.01	0.03	0.02	0.03	-0.04	-0.01	-0.01	-0.02	-0.05
5:00	0	-0.04	-0.03	0.03	0.01	0.01	-0.04	-0.02	-0.01	-0.03	-0.06
6:00	-0.04	-0.05	-0.06	0	-0.01	-0.02	-0.03	-0.06	0.01	-0.04	-0.09
7:00	-0.04	-0.03	-0.06	-0.02	0.01	-0.04	-0.01	-0.07	0.02	-0.03	-0.1
8:00	-0.01	-0.02	-0.04	-0.01	0.04	-0.02	0	-0.04	0.02	-0.03	-0.08
9:00	-0.06	-0.07	-0.1	-0.05	0	-0.08	-0.06	-0.1	-0.04	-0.09	-0.15
Daily	**-0.065**	**-0.135**	**-0.180**	**-0.013**	**-0.059**	**-0.079**	**-0.140**	**-0.118**	**-0.144**	**-0.183**	**-0.196**

In Table 5.6, the hourly mean temperature changes for each mitigation scenarios for non built-up area are summarized. The last row of this table represents the daily differences of these scenarios and the red boxes indicate the most significant values. The mean cooling effect of the green roofs amounts to 0.013K and 0.059K for 30% and 70%, respectively.

The increase in the albedo of the walls and the buildings leads to temperature changes of -0.065K, -0.135K and -0.180K, which is about 3 to 6 times the effect of the green roofs. However, the cooling effect of the white and green scenarios for non built-up areas has considerably low values in comparison with the values of built-up areas. As is the case with the previous Table 5.4, the combination of these scenarios which is represented by “Hybrid 6” has less cooling effect then the total amount of the “White 3” and “Green 2”, since the effectiveness of the cool roofs are higher separately so combining this scenario with the greenery reduced the mitigation potential of them. On the other hand, the daily value of “Hybrid 5” is so close to “Hybrid 6” although the “grant” (green roof fraction) parameter of “Hybrid 5” is 0.4 less then the “Hybrid 6”s.

Since having more considerable daily temperature anomalies, “White 3”, “Green 2”, “Hybrid 5” and “Hybrid 6” will be investigated in more detail in the forthcoming parts. Besides, the analyses of the rest of the scenarios will be attached in the Appendix.

5.3.1.2 Spatial distribution of the temperature changes

To observe the impact of the mitigation strategies in the whole simulation area, the spatial distribution of the 2 m temperature differences will be shown. Thus, the four mitigation strategies (White 3, Green 2, Hybrid 5, Hybrid 6), which were indicated in the former section, have been selected. The green and white simulations will be shown first, and the hybrid simulations afterwards.

In Figure 5.19 and Figure 5.20, the simulated temperature differences for the one green, one white and two hybrid scenarios are shown, respectively. Clearly, the higher the mitigation parameters, the higher the temperature changes in other words “Hybrid 6” scenario. Moreover, the main effects of mitigation strategies can be seen in built-up areas, which is due to the fact that the changes only take place on land use class no. 1 to16, in short on buildings. The cooling effects do not show a significant difference on non built up areas, which can be seen in the small white grid points in the city.

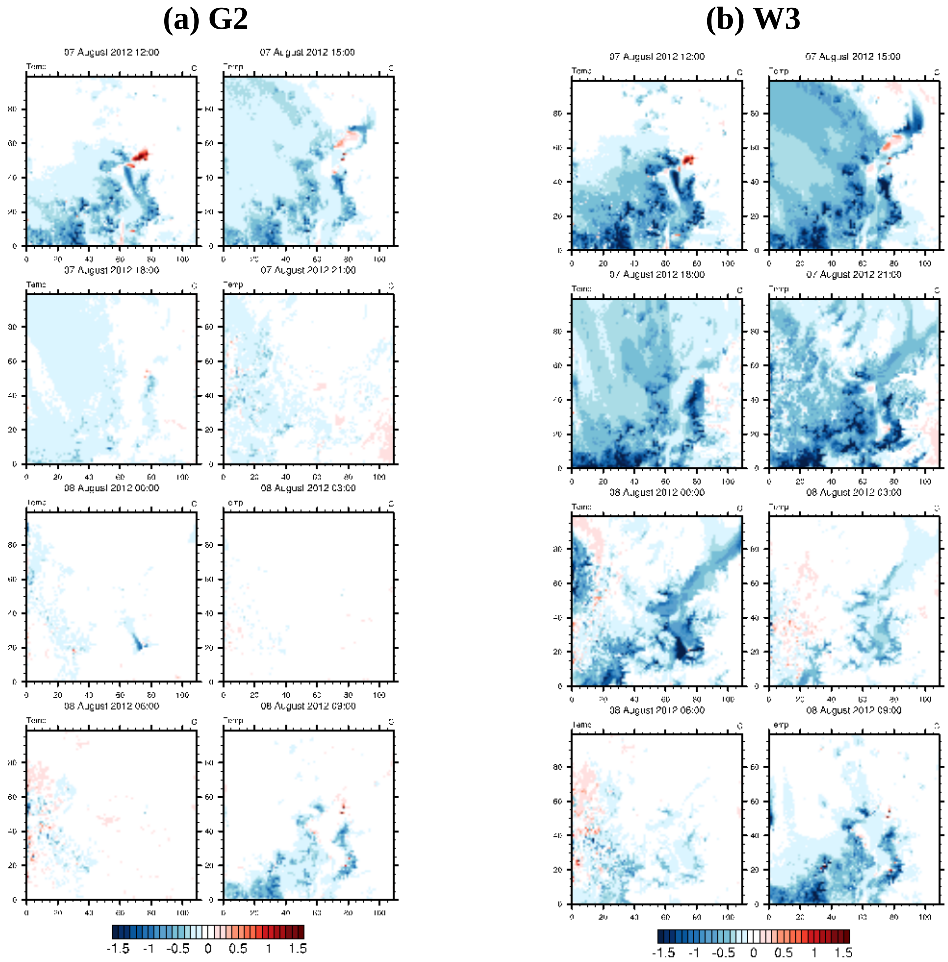

Figure 5.19 : Spatial distribution of green 2 **(a)** and white 3 **(b)** scenerios.

Furthermore, Figure 5.19 and Figure 5.20 also emphasizes that the simulation results with the mitigation scenarios show that cool roofs (White 3) are more effective than green roofs (Green 2), which could also be seen in Figure 5.16. Clearly, the combination of green roofs and high-albedo materials have more effect than each of them on their own, although the changes are not as striking as expected.

The distribution of the nighttime temperature changes in the figures is similar to daytime changes, although the effects seem to be blurred and, the cooling effect of the rural areas is low especially for the 21:00, 00:00 and 03:00 simulations. In Figure 5.19 and Figure 5.20, the effect of each land use class can be seen very clearly, especially considering the residential area.

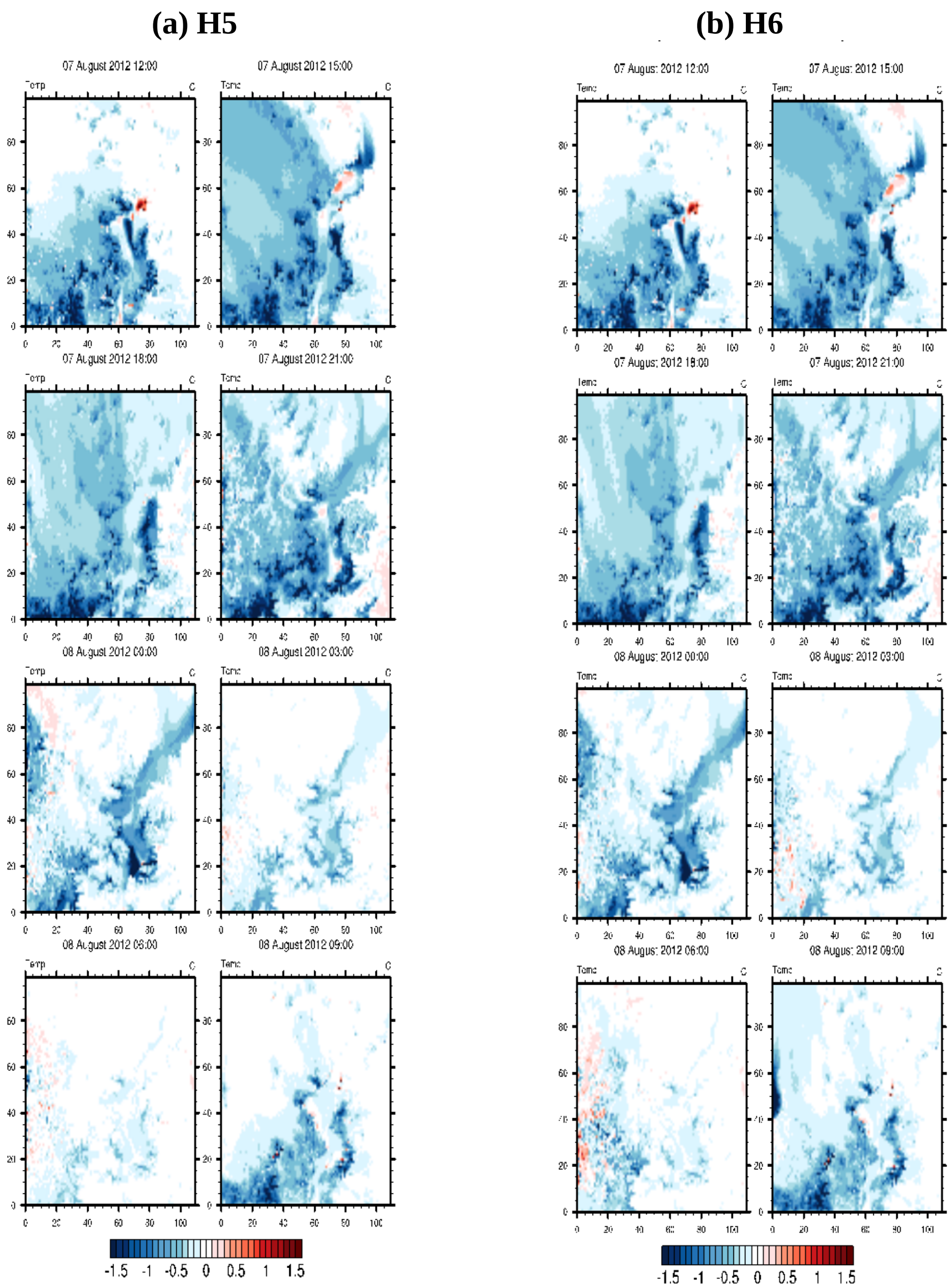

Figure 5.20 : Spatial distribution of hybrid 5 **(a)** and hybrid 6 **(b)** scenerios.

In Figure 5.21 and Figure 5.22, the parameter changes for roofs and walls are only applied for areas with high-rise buildings (no. 4, 8, 12 and 16 in the land use table) and the simulated temperature differences between scenarios and the reference run for the one green, one white and two hybrid simulations are shown, respectively.

As it was shown in the previous figures (Figure 5.19 and Figure 5.20**)**, the considerable effects of mitigation strategies can be seen in built-up areas, which is due to the fact that the changes only take place on land use class no. 1 to16, in short on buildings but for this time the case is more specific and the significant changes for the high-rise buildings can be observed easily.

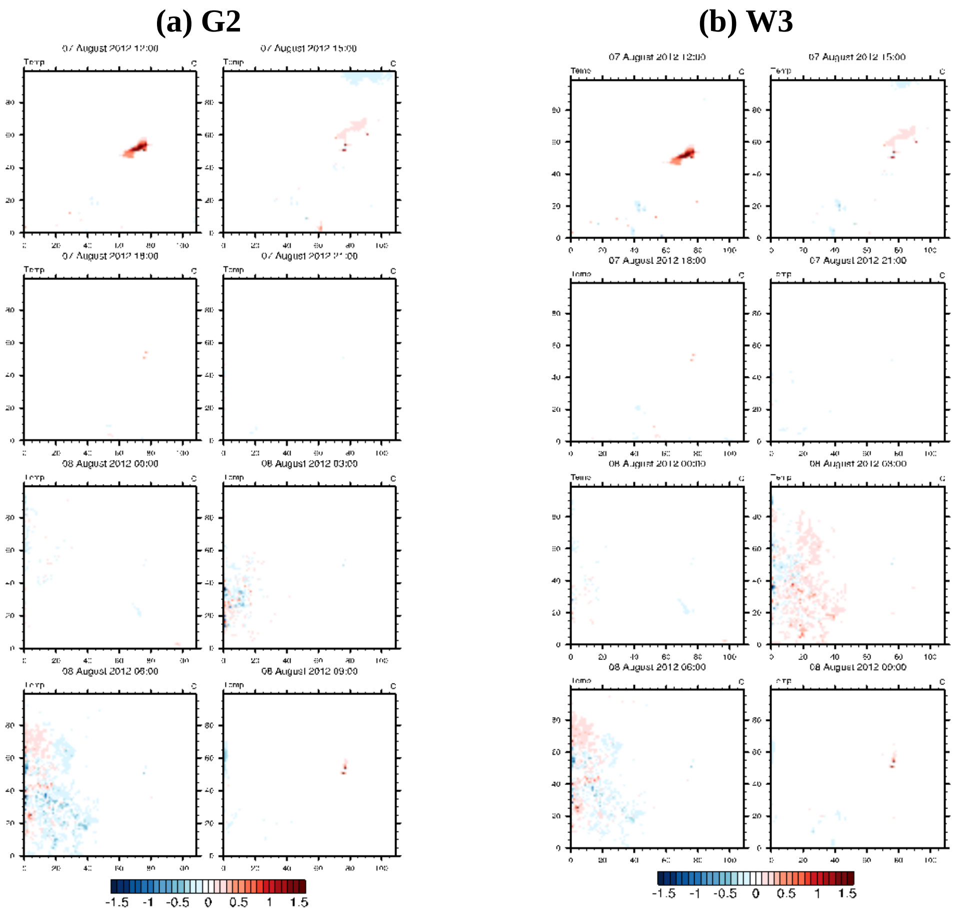

Figure 5.21 : Spatial distribution of green 2 **(a)** and white 3 **(b)** scenerios for high-rise built-up area.

Furthermore, Figure 5.21 and Figure 5.22 also emphasizes that the simulation results with the mitigation scenarios show that cool roofs (White 3) and hybrids are more effective than green roofs (Green 2), which could also be seen in Figure 5.16**,** Figure 5.19 and Figure 5.20.

This time the distribution of the nighttime temperature changes in the figures are not similar to daytime changes. There are significant warming effects especially for the noontime temperatures for all scenarios, almost none cooling or warming effects for the 15:00, 18:00, 21:00 and 00:00 simulations but there are blurred warming effect around 03:00 especially for “White 3” and “Hybrid 6”. The interesting part is, there are warming effect for the forested area and cooling effect for the residential area around 06:00 for the “Green 2”, “White 3” and “Hybrid 6” scenarios but there is only warming effect around 06:00 for the “Hybrid 5” scenario although this scenario generally gives similar results to “Hybrid 6”.

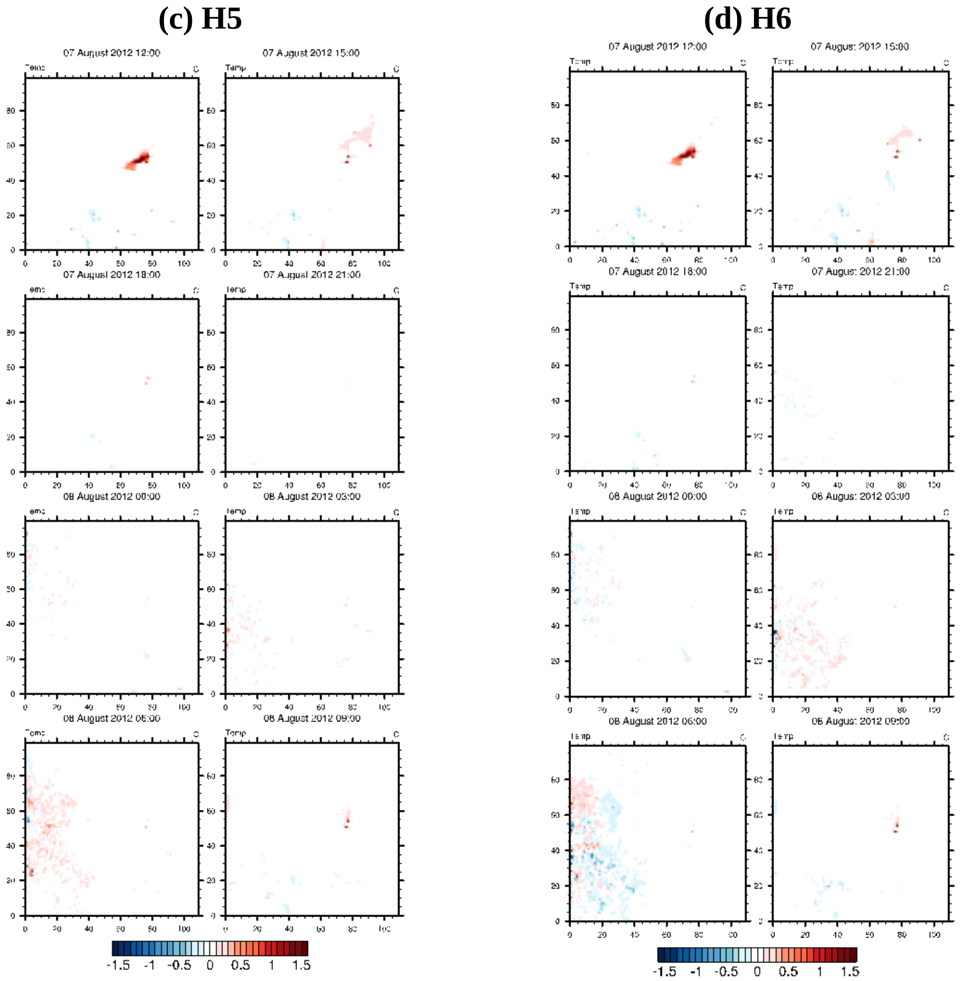

Figure 5.22 : Spatial distribution of hybrid 5 **(a)** and hybrid 6 **(b)** scenerios for high-rise built-up area.

In Figure 5.23 and Figure 5.24, the parameter changes for roofs and walls are only applied for areas with high density built-up area (no. 13, 14, 15 and 16 in the land use table) and the simulated temperature differences between scenarios and the reference run for the one green, one white and two hybrid simulations are shown, respectively.

As it was shown in the previous figures (Figure 5.19 and Figure 5.20**)**, the considerable effects of mitigation strategies can be seen in built-up areas, which is due to the fact that the changes only take place on land use class no. 1 to16, in short on buildings but for this time the case is more specific and the significant changes for the high density residential area can be observed easily.

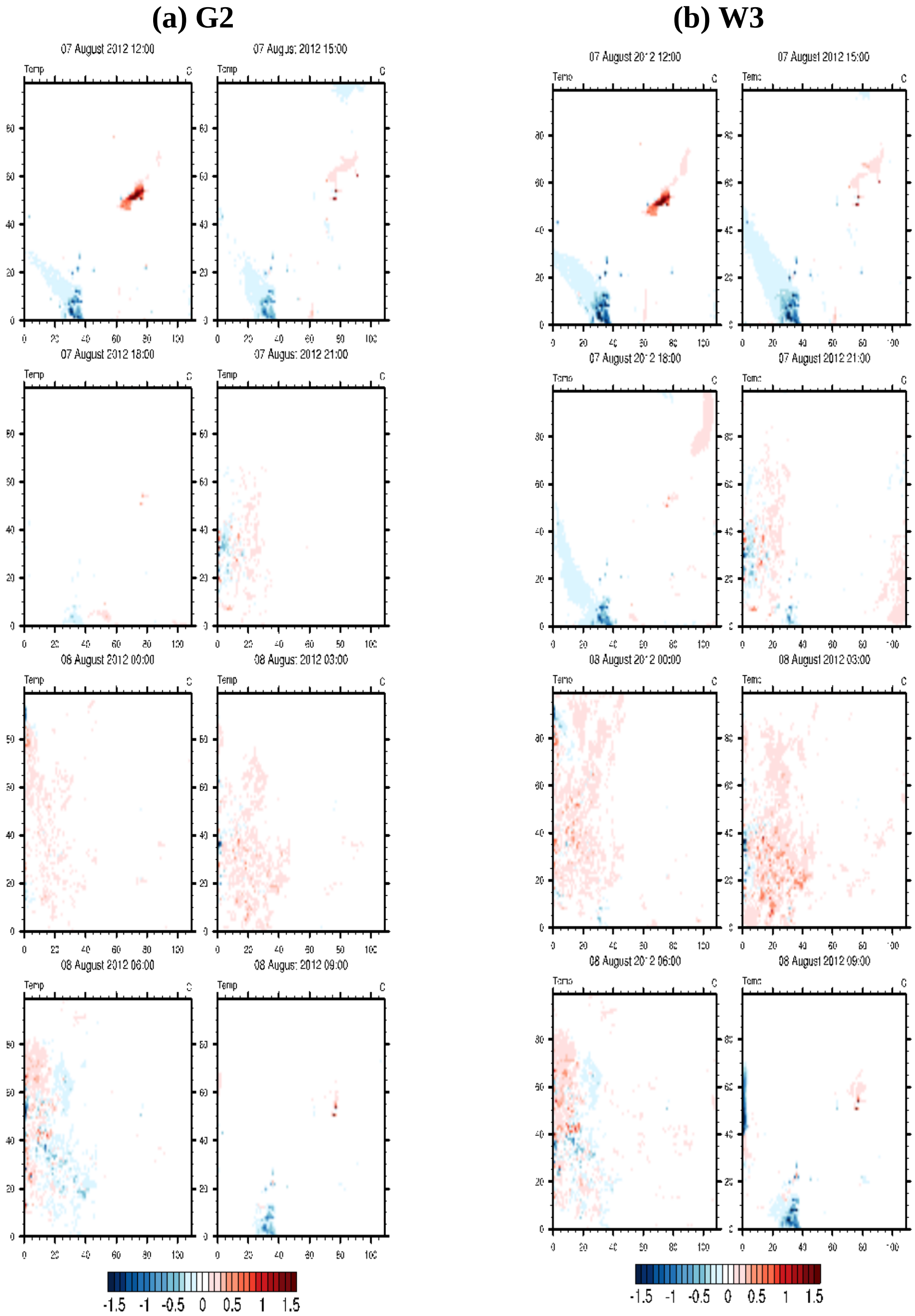

Figure 5.23 : Spatial distribution of green 2 **(a)** and white 3 **(b)** scenerios for high-density built-up area.

Figure 5.23 and Figure 5.24 also emphasizes that the simulation results with the mitigation scenarios show that “White 3”, “Hybrid 5” and “Hybrid 6” are more effective than “Green 2” again, which could also be seen in Figure 5.16**,** Figure 5.19 and Figure 5.20.

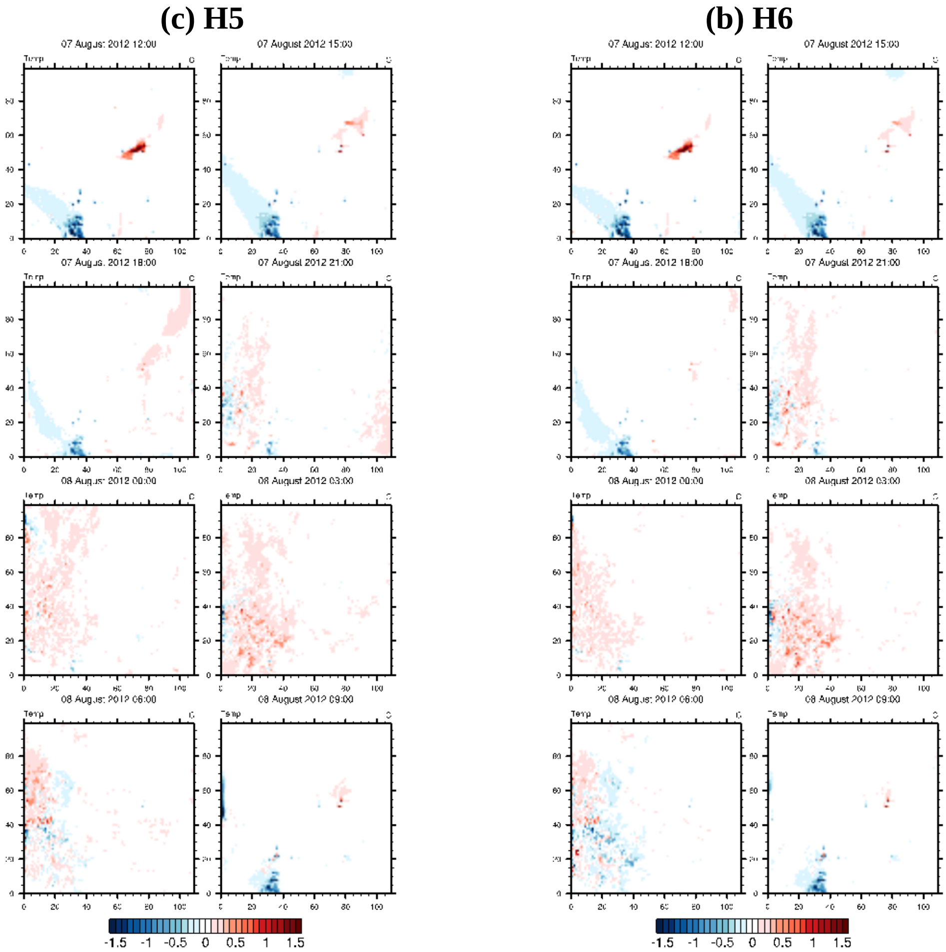

Figure 5.24 : Spatial distribution of hybrid 5 **(a)** and hybrid 6 **(b)** scenerios for high-density built-up area.

As is the case with high-rise building simulations, the distribution of the nighttime temperature changes in the figures are not similar to daytime changes. There are significant warming effects for the high density residential area with high-rise buildings whereas considerable cooling effect for high density built-up area with low and medium height buildings and traffic area especially for the noontime, sectional warming effects for forested and agricultural area around 00:00 and 03:00, and blurred warming effects around 06:00 for all The interesting part is, there are warming effect for the forested area and cooling effect for the residential area around 06:00 for all scenarios .

6. CONCLUSION

The UHI effect is exhibited by the mega cities in the world because of the built-up areas experienced higher temperatures than surrounding areas. In this study, results from UHI effect are summarized as; in recent decades, Istanbul as the one of the mega cities has exposed to significant urban heat island due to the rapid urbanization. During summer period, the UHI takes its maximum intensity between Kartal (urban) and Şile (suburban) sites of the city. The average difference for the whole measurement period is 3.01K.

Governments, urban planners and urban residents are seeking practical approaches to improve urban heat mitigation at least cost as adaptation to global warming, extreme heat events and urban heat effects. In this thesis, the micro-scale urban climate model MUKLIMO_3 has been used for the implementation of mitigation strategies in order to reduce the urban heat island effect and the most populated city of Turkey, Istanbul, was chosen for this.

MUKLIMO_3 is a new model, which has not been used and, validated sufficiently for mega city Istanbul until now and it is able to simulate mitigation strategies, and thus could be a great opportunity for urban planners to optimize their cities with regard to urban heat island. Once initialised for a city properly, different mitigation strategies such as high albedo materials or more vegetative area and new building structures can be implemented and calculated.

With the roof treatments explored here, results suggest that the high albedo rooftop, if combined with greenery, would probably provide the greatest overall benefit in terms of urban heat mitigation strategy and heat transfer into buildings. Our results suggest that irrigation is necessary for green roofs to provide a substantial daytime microclimate benefit, because, under dry conditions, Q_E was low and Q_H was high. Green roofs could provide sufficient benefits and be effective solutions like cool roofs if they are regularly irrigated and planted with a dense mix of actively transpiring vegetation.

REFERENCES

Ayata, T., Tabares-Velasco, P. C., & Srebric, J. (2011). An investigation of sensible heat fluxes at a green roof in a laboratory setup. Building and Environment; 46: 1851e61.

Blackadar, A. K. (1962). The vertical distribution of wind and turbulent exchange in a neutral atmosphere. J. Geophys. Res. 67, 3095-3102.

Böhm, R. (1998). Urban bias in temperature time series: a case study for the City of Vienna, Austria. Clim. Change 38, 113–128.

Chen, Y., & Wong, N. H. (2009). Thermal impac to fstrategic landscaping in cities: are view. Advances in Building Energy Research;3:237e60.

Coutts, A. M., Daly, E., Beringer, J. & Tapper, N. J. (2013). Assessing practical measures to reduce urban heat: green and cool roofs *Build. Environ.* 70 266–76

Früh, B., Becker, P., Deutschländer, T., Hessel, J.-D., Koßmann, M., Mieskes, I., Namyslo, J., Roos, M., Sievers, U., Steigerwald, T., Turau, H., & Wienert, U. (2011). Estimation of climate change impacts on the urban heat load using an urban climate model and regional climate projections, Journal Applied Meteorology and Climatology, 50(1), 167-184

Giannaros, T. M., Melas, D., Daglis, I. A., Keramitsoglou, I., & Kourtidiset, K. (2013). Numerical study of the urban heat island over Athens (Greece) with the WRF model, Atmospheric Environment 73, 103-111.

Gabriel, K. M. & Endlicher, W. R. (2011). Urban and rural mortality rates during heat waves in berlin and brandenburg, germany. *Environmental pollution*, 159(8), pp. 2044–2050.

Getter, K. L., Rowe, D. B., Andresen, J. A., & Wichman, I. S. (2011). Seasonal heat flux properties of an extensive green roof in a Midwestern U.S. climate. Energy and Buildings;43:3548e57.

Gross, G. (1989). Numerical simulation of the nocturnal flow systems in the Freiburg area for different topographies. Beiträge zur Phys. Atmos. 62, 57–72

Gutman, D. P. & Torrance, K. E. (1975). Response of the urban boundry layer to heat addition and surface roughness. Boundry-Layer Meteor. 9, 217-233.

Harlan, S. L., Declet-Barreto, J. H., Stefanov, W. L., & Petitti, D. B. (2011).

Neighborhood effects on heat deaths: social and environmental predictors of vulnerability in maricopa county, arizona. *Environmental health perspectives*, 121(2), pp. 197–204.

Henderson-Sellers, A. (1993). A factorial assessment of the sensitivity of the BATS land-surface parameterization scheme, *J. Climate* 6, 227–247.

IBB. (2015). http://www.ibb.gov.tr/tr-tr/kurumsal/pages/ilceveilkkademe.aspx, İstanbul Greater Istanbul Districts, Retrieved 2015-01-15.

IPCC. (2013). Climate Change 2013: The Physical Science Basis. Contribution of Working Group I to the Fifth Assessment Report of the Intergovernmental Panel on Climate Change, Stocker, T. F., Qin, D., Plattner, G. K., Tignor, M., Allen, S. K., Boschung, J., Nauels, A., Xia, Y., Bex, V., & Midgley P. M. (eds.), Cambridge University Press, Cambridge, United Kingdom and New York, NY, USA.

Ishigami, A., Hajat, S., Kovats, R. S., Bisanti, L., Rognoni, M., Russo, A., & Paldy, A. (2008). An ecological time-series study of heat-related mortality in three european cities. *Environ Health*, 7(5), pp. 1–7.

Jendritzky, G. Folgen des klimawandels für die gesundheit. 2007.

Kniebush, M. S., & Hajat, S. (2008). Heat stress and public health: a critical review. *Annu. Rev. Public Health*, 29, pp. 41–55.

Karaca, M., Anteplioglu, U., & Karsan, H. (1995). Detection of urban heat island in Istanbul, Turkey. *Nuovo Cimento- Societa Italiana di Fisica Sezione C*, 18(1):49-55 · January.

Kovats, R. S., &Hajat, S. (2008). Heat stress and public health: a critical review. *Annu. Rev. Public Health*, 29, pp. 41–55.

Landsberg, H.E. (1981). The Urban Climate, Int. Geophys. Ser., Vol. 28, Academic Press, New York, p. 275.

Lin, C. Y., Chen, F., Huang, J. C., Chen, W. C., Liou, Y. A., Chen, W. N., & Liu, S. C. (2008). Urban heat island effect and its impact on boundary layer development and land–sea circulation over northern Taiwan, Atmospheric Environment, 42, 5635-5649.

Oke, T. R. (1973). City size and the urban heat island. *Atmospheric Environment (1967)*, 7(8), pp. 769–779.

Oke, T. R. (1982). The energetic basis of the urban heat island. Q. J. R. Meteorol. Soc. 108, 1–24.

Oke, T. R. (1987). *Boundary Layer Climates*, volume 5. Psychology Press.

Pankart, J. (1975). Numerische modellierung der substanz und warmeausbreitung in der wirbelströmung in einer gelandevertiefung. Beitr. Phys. Atmosph. 48, 327-348.

Priyadarsini, R., Hien, W. N., & David, C. K. W. (2008). Microclimatic modeling of the urban thermal environment of Singapore to mitigate urban heat island, Solar Energy, 92, 727–745

Rosenfeld, A. H., Akbari, H., Romm, J. J., & Pomerantz, M. (1998). Cool communities: strategies for heat island mitigation and smog reduction. Energy and Buildings 1998;28: 51e62.

Santamoris, M. (2014). Cooling the cities – A review of reflectivity and green roof mitigation technologies to fight heat island and improve comfort in urban environment, Solar Energy, 103,682-703.

Sarrat, C., Lemonsu, A., Masson, V., & Guedalia, D. (2006). Impact of urban heat island on regional atmospheric pollution, Atmospheric Environment, 40, 1743-1758

Scherba, A., Sailor, D. J., Rosenstiel, T. N. , & Wamser, C. C. (2011). Modeling impacts of roof reflectivity, integrated photovoltaic panels and green roof systems on sensible heat flux into the urban environment. Building and Environment; 46: 2542e51.

Siebert, J., Sievers, U., & Zdunkowski, W. (1992). A one-dimensional simulation of the interaction between land surface processes and the atmosphere. Boundary-Layer Meteorology 59, p. 1-34.

Sievers, U. (1995). Verallgemeinerung der Stromfunktionsmethode auf drei Dimensionen (Generalization of the streamfunction– vorticity method to three dimensions). Meteor. Z., 3, 3–15.

Sievers, U., & Zdunkowski, W. (1986). A microscale urban climate model. Contrib. Atmos. Phys., 59, 13–40.

Sievers, U., Forkel, R., & Zdunkowski, W. (1983). Transport equations for heat and moisture in the soil and their application to boundary layer problems. Beitr. Phys. Atmosph. 56, p. 58-83.

Sievers, U., Mayer, I., & Zdunkowski, W. (1987). Numerische Simulation des urbanen Klimas mit einem zweidimensionalen Modell, Meteorol. Rundschau 40(1 and 3), 40–52 and 65–83

Sievers, U., & Früh, B. (2012). A practical approach to compute short-wave irradiance interacting with subgrid-scale buildings. Met. Zeit. 21, 349-364

Sievers, U. (2012). *Das kleinskalige Strömungsmodell MUKLIMO_3 Teil 1: Theoretische Grundlagen, PC- Basisversion und Validierung (2. Entwurf, Stand: 02/2014*. Selbstverlag des Deutschen Wetterdi- enstes, Offenbach am Main.

Sodoudi, S., Shahmohamadi, P., Vollack, K., Cubasch, U., & Che-Ani, A. (2014). Mitigating the urban heat island effect in megacity tehran. *Advances in Meteorology*.

Solomon, S., Qin, D., Manning, M., Marquis, M., Averyt, K., Tignor, M. M. B.,

Miller Jr. H. L., & Chen, Z. (2007). Climate Change 2007: The Physical Science Basis. Cambridge University Press, 996 pp.

Souch, C., & Grimmond, C. S. B. (2004).: Applied climatology: 'Heat waves.' Prog. Phys. Geogr., 28, 599–606.

Stewart, I. D. (2011). A systematic review and scientific critique of methodology in modern urban heat island literatüre, International Journal of Climatology, 31, 200–217,

Sun, R., Chen, A., Chen, L., & Lü, Y. (2012). Cooling effects of wetlands in an urban region: The case of Beijing Ecological Indicators, 20, 57-64

Susca, T. (2011). Urban-wide change in albedo: a multi-scale approach to LCA. The case study of New York City. *SETAC Europe 21st Annual Meeting*. Milano.

Synnefa, A., Dandou, A., Santamouris, M., Tombrou, M., & Soulakellis, N. (2008). On the use of cool materials as a heat island mitigation strategy. Journal of Applied Meteorology and Climatology 2008;47:2846-56.

Takebayashi, H., & Moriyama, M. (2007). Surface heat budget on green roof and high reflection roof for mitigation of urban heat island. Building and Environment 2007;42:2971e9.

Unal, Y. S., Tan, E., & Mentes, S. S. (2013). Summer heat waves over western Turkey between 1965 and 2006. *Theor Appl Climatol* 112:339–350

United Nations Report. (2014). World urbanization prospects, the 2014 revision. *United Nations, Department of Economic and Social Affairs, New York.*

Vardoulakis, E., Karamanis, D., Fotiadi, A., & Mihalakakou, G. (2013). The urban heat island effect in a small Mediterranean city of high summer temperatures and cooling energy demands, Solar Energy, 94, 128-144.

Velazquez-Lozada. A., Gonzalez, J.E., & Winter, A. (2006). Urban heat island effect analysis for San Juan, Puerto Rico. Atmospheric Environment. 40, 1731-1741

Yalcin, T., & Yetemen, O. (2009). Local warming of groundwater caused by the urban heat island effect in Istanbul, Turkey. *Hydrogeology Journal:* 17, 1247–1255.

Wu, S. S. (1965). Astudy of heat transfer coefficients in the lowest 400 meters of atmosphere. J. Geophys. Res. 70, 1801-1807.

Zaitchic, B. F., Macalady, K. A., Bonneau, L. R., & Smith, R. B. (2006). Europe's 2003 heat wave: a satellite view of impacts and land–atmosphere feedbacks, Int. J. Climatol. 26 743–769

Žuvela-Aloise, M., Hollosi, B., Weyss, G., & Löffelmann, P. (2015). Evaluating urban climate model simulations with low-cost air temperature measurements. ICUC9.

CURRICULUM VITAE

Name Surname	**:**	Simge Irem Bilgen
Place and Date of Birth	**:**	İZMİR 12/01/1991
E-Mail	**:**	simgebilgen@gmail.com

EDUCATION **:**

- **B.Sc.** **:** 2014, Istanbul Technical University, Faculty of Aeronautics and Astronautics, Meteorological Engineering

PROFESSIONAL EXPERIENCE AND REWARDS:

- 2014-2016 European Union Project, ERANET, LOCLIM3-Local climate change in 3 cities: Cairo, Nairobi, Istanbul, funded by TUBITAK (The Scientific and Technological Research Council of Turkey)
- 2014-2015 Turkish Ministry of Forestry and Water Affairs Project, Hydrometeorological Projections for Tigris-Euphrates Basin, Republic of Republic of Turkey Ministry of Forestry and Water Affairs, Republic of Turkey Water Institute Hydro-meteorological Report
- 2015-2016 General Directorate of Water Management Project, Impact of Climate Change on Water Resources over 25 Basin of Turkey

PUBLICATIONS, PRESENTATIONS AND PATENTS:

- **Bilgen S.I.**, Balli C., Unal Y.S., *"Assessment of Regional Climate Model (RegCM) Simulations for High and Low Resolutions over Turkey between 1971-2000: Temperature and Precipitation"*, 14th EMS Annual Meeting & 10th European Conference on Applied Climatology (ECAC), October, 2014, Prague, Czech Republic

• **Bilgen S.I.**, Yuruk,C., Unal Y.S., *"Variability of Regional Climate Model (RegCM) Simulations for High And Low Resolutions Over Turkey Between 1971-2000: Temperature And Precipitation"*, Climate Change and Climate Dynamics Conference (CCCD), October, 2014, Istanbul, Turkey

• Yuruk,C, **Bilgen S.I.**, Unal Y.S., Incecik S., "*Inter annual Variations of Precipitation and Temperature Observations in Turkey"*, 5th International Conference on Meteorology and Climatology of the Mediterranean (METMED), March, 2015, Istanbul, Turkey

• **Bilgen, S.I.,** Yuruk, C., Goktepe, N., Tan, E., And Unal, Y.S., "*Investigation on Heat Waves Over Turkey and Leading Atmospheric Patterns*", 5th International Conference on Meteorology and Climatology of the Mediterranean (METMED), March, 2015, Istanbul, Turkey

• Unal, Y., **Bilgen S.I.**, Yürük C., Langer I., El Zafarany A.M., Diren D., İncecik S., Topcu S., Abou El Seoud T., Güney C., Dogru A.Ö., Wesonga J.M., "*ERAfrica Project: LOCLIM3- The local climate changes in 3 cities of Cairo, Nairobi and İstanbul: İstanbul Case",* 7th Atmospheric Sciences Symposium (ATMOS), March, 2015, Istanbul, Turkey

• **Bilgen S.I.**, Yürük C., Unal, Y., Goktepe N., İncecik S., Topcu S., Abou El Seoud T., Güney C., Dogru A.Ö., *"Investigation of Urban Heat Island Intensity in Istanbul"*, European Geosciences Union (EGU) General Assembly 2016, April, 2016, Vienna, Austria

• Yürük C., Unal, Y., **Bilgen S.I.**, Topcu S., Mentes S., *"Determining Heat Waves from Observations and COSMO-CLM Simulations in Istanbul"*, European Geosciences Union (EGU) General Assembly 2016, April, 2016, Vienna, Austria